



Mass spectrometric characterization of the seco acid formed by cleavage of the macrolide ring of the algal metabolite goniiodomin A

Constance M. Harris^a, Luisa Hintze^b, Sylvain Gaillard^c, Simon Tanniou^d, Hamish Small^c, Kimberly S. Reece^c, Urban Tillmann^b, Bernd Krock^b, Thomas M. Harris^{a,*}

^a Department of Chemistry, Vanderbilt University, Nashville, TN, 37235, USA

^b Alfred Wegener Institut-Helmholtz Zentrum für Polar- und Meeresforschung (AWI), 27570, Bremerhaven, Germany

^c Department of Aquatic Health Sciences, Virginia Institute of Marine Science (VIMS), William & Mary, Gloucester Point, VA, 23062, USA

^d Ifremer, PHYTOX, Laboratoire METALG, F-44000, Nantes, France

ARTICLE INFO

Handling Editor: Ray Norton

Keywords:

Alexandrium toxins
Mass spectrometry
Retro-Diels-Alder fragmentation
Endotoxin: Goniiodomin A (GDA)
Exotoxin: Seco acid (GDA-sa)
Alkyl-O cleavage

ABSTRACT

Goniiodomin A (GDA) is a polyketide macrolide produced by multiple species of the marine dinoflagellate genus *Alexandrium*. GDA is unusual in that it undergoes cleavage of the ester linkage under mild conditions to give mixtures of seco acids (GDA-sa). Ring-opening occurs even in pure water although the rate of cleavage accelerates with increasing pH. The seco acids exist as a dynamic mixture of structural and stereo isomers which is only partially separable by chromatography. Freshly prepared seco acids show only end absorption in the UV spectrum but a gradual bathochromic change occurs, which is consistent with formation of α,β -unsaturated ketones. Use of NMR and crystallography is precluded for structure elucidation. Nevertheless, structural assignments can be made by mass spectrometric techniques. Retro-Diels-Alder fragmentation has been of value for independently characterizing the head and tail regions of the seco acids. The chemical transformations of GDA revealed in the current studies help clarify observations made on laboratory cultures and in the natural environment. GDA has been found to reside mainly within the algal cells while the seco acids are mainly external with the transformation of GDA to the seco acids occurring largely outside the cells. This relationship, plus the fact that GDA is short-lived in growth medium whereas GDA-sa is long-lived, suggests that the toxicological properties of GDA-sa in its natural environment are more important for the survival of the *Alexandrium* spp. than those of GDA. The structural similarity of GDA-sa to that of monensin is noted. Monensin has strong antimicrobial properties, attributed to its ability to transport sodium ions across cell membranes. We propose that toxic properties of GDA may primarily be due to the ability of GDA-sa to mediate metal ion transport across cell membranes of predator organisms.

1. Introduction

The dinoflagellate genus *Alexandrium* is globally distributed in the marine world (Anderson et al., 2012). Approximately half of the numerous formally described *Alexandrium* species are known to produce characterized toxins which are distributed among three classes: 1) saxitoxins, 2) spirolides and gymnodimines and 3) alexandrolides and goniiodomins (GDs) (Long et al., 2021). The saxitoxins are small

neurotoxic metabolites that have been the subject of extensive study due to their high toxicity. Spirolides and gymnodimines are macrocyclic imines and alexandrolides; goniiodomins are macrolides. The primary GD is goniiodomin A (GDA, 1). GDA-producing *Alexandrium* species are found in estuarine waters throughout much of the world. Four of these species are known: *A. hiranoi*, *A. pseudogonyaulax*, *A. monilatum* and *A. taylorii* (Murakami et al., 1988a,b; Hsia et al., 2006; Zmerli Triki et al., 2016; Tillmann et al., 2020).

Abbreviations: DFT, Density Function Theory.

* Corresponding author.

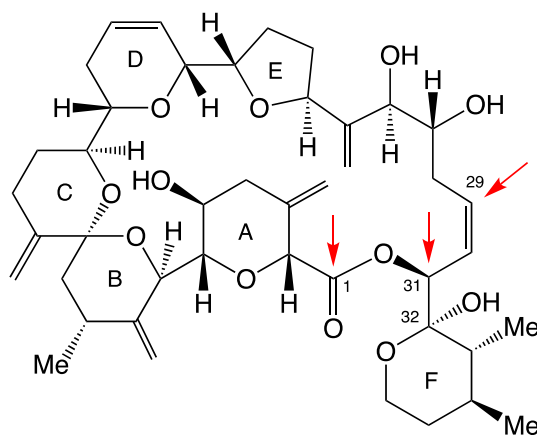
E-mail address: thomas.m.harris@vanderbilt.edu (T.M. Harris).

<https://doi.org/10.1016/j.toxicon.2023.107159>

Received 8 February 2023; Received in revised form 10 May 2023; Accepted 11 May 2023

Available online 18 May 2023

0041-0101/© 2023 Elsevier Ltd. All rights reserved.

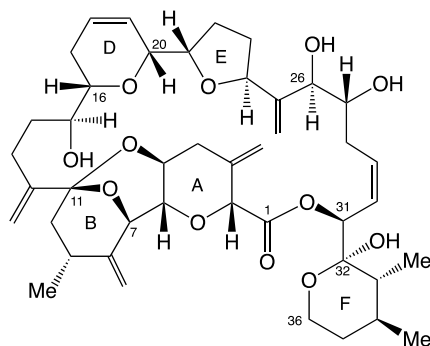


GDA (1, Red arrows denote potential sites of hydrolytic attack.)

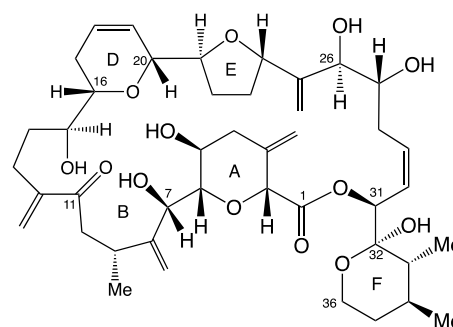
GDA was first isolated by Burkholder and coworkers more than half a century ago from a large bloom of an unidentified *Alexandrium* species on the coast of Puerto Rico (Sharma et al., 1968). The structure of GDA, including stereochemistry and absolute configuration, were established by Murakami and Takeda using spectroscopic and chemical means (Murakami et al., 1988a,b; Takeda et al., 2008) but there has been speculation (Kawashima, 2018) that an error might have been made in configurational assignments. Major efforts have been made to confirm Takeda's structure by total synthesis (Fujiwara et al., 2007; Katagiri et al., 2008a,b; Saito et al., 2009; Fuwa et al., 2011, 2016; Nakajima, 2014; Kawashima, 2018). The synthetic efforts have not yet been successful but we have confirmed the structure by X-ray crystallography

GDA is difficult to work with because it degrades under mild conditions (Onofrio, 2020). LC-MS analyses of phycotoxins are frequently carried out under acidic and basic conditions, used to improve ionization efficiency. GDA degrades under both, creating a frustrating conundrum as to how best to carry out quantitative analyses. Onofrio et al. (2020) reported that acidic conditions gave poor peak shapes and produced multiple peaks on LC-MS. We subsequently explored the instability of GDA in acid and found that equilibration occurs with an isomer (goniodomin B, GDB, 2) and an α,β -unsaturated ketone (goniodomin C, GDC, 3), with the latter resulting from hydrolysis of the spiroketal (Harris et al., 2021).

A second pathway of degradation involves the cleavage of the ester



GDB (2)



GDC (3)

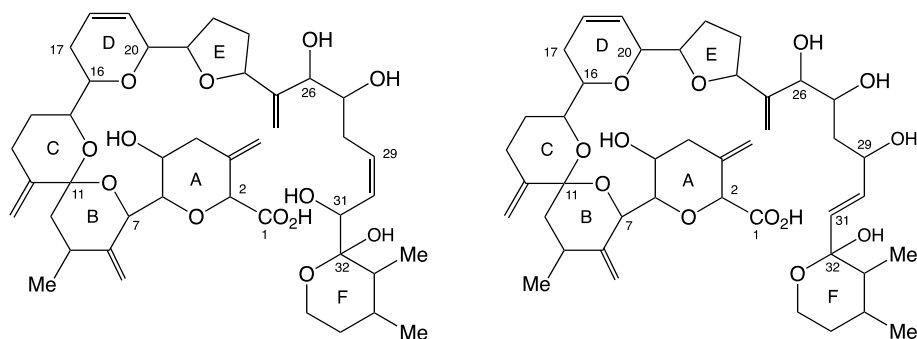
(Tainter et al., 2020).

The toxicity of GDA-producing species had been studied for many years (Connell and Cross, 1950; Howell, 1953; Gates and Wilson, 1960; Harding et al., 2009; May et al., 2010) but those studies did not link GDA to observed toxicity. The toxic effects of GDA itself have also been investigated and have been attributed to interactions with actin (Mizuno et al., 1998; Yasuda et al., 1998; Matsunaga et al., 1999; Abe et al., 2002; Furukawa et al., 1993; Espiña et al., 2016). It is not clear that the toxicity observed with purified GDA is as great as that observed with cells. Overall, the toxicity of GDA has received insufficient attention due to poor availability and lack of evidence for human toxicity.

The question can be raised of whether other metabolites are the actual source of observed toxicity in GDA-producing *Alexandrium* spp. For some *Alexandrium* species the presence of as yet unidentified extracellular toxins has been observed (Tillmann and John, 2002; Ma et al., 2009; Long et al., 2021). In summary, the ecological role of GDA in the marine environment remains to be discovered.

This pathway is most pronounced under basic conditions. Onofrio (2020) observed that degradation occurred even in pure water but significantly faster in seawater where the pH is approximately 8. The extent of GDA degradation in water and seawater was reported to be 43% and 93%, respectively, within 6 h. Structures of the degradation products were not examined. At the other extreme, Takeda et al. (2008) had earlier failed to cleave the lactone of GDA using methanolic K_2CO_3 , ascribing his failure to steric hindrance. The present paper addresses degradations of GDA involving cleavage of the ester linkage under alkaline conditions to form seco acids (GDA-sa). This process occurs at all pH values that have been studied, although ester cleavage under acidic conditions is slow compared to formation of GDB and GDC. Hydrolysis of the ester linkage of GDA by attack at C1 and C31 would yield GDA-sa-1 (4a). Cleavage by allylic attack at C29 would yield GDA-sa-2 (4b). 4a and 4b are collectively referred to in this paper as GDA-sa (4). The three potential attack sites are indicated by red arrows on structure 1.

The aim of this study is to clarify the chemistry of GDs in order to lay



GDA-sa-1 (4a) GDA-sa (4b) Note: Center 4a and 4b under the two structures.

the groundwork for assessment of the harmful effects of GD-producing microalgal species, which have been associated with fishkills and possibly pose a risk for marine biodiversity and human health. Yet, little is known about GD-producing species, the role of GDs in fishkills, and about conversions of GDs in the natural environment. This work tries to fill the knowledge gap to facilitate future work on toxicological assessment and evaluation of the ecological effects of GDA-sa and other GDs in the marine environment.

2. Methods

2.1. Materials

GDA was isolated by the previously described procedure from *A. monilatum* cells that had been collected via plankton nets from natural blooms in the York River, VA, USA (Harris et al., 2020a). The procedure for isolation of GDA and GDA-sa from field samples of *A. pseudogonyaulax* used previously published methodology (Krock et al., 2018) with modifications in sample handling to minimize formation of GDB and GDC (Hintze, 2021). MeOH and other solvents used for reactions were ACS grade. HPLC analyses and separations were carried out with chromatography grade reagents. Reagents for MS and LC-MS analyses were mass spectrometry grade. Milli-Q deionized water was employed for reactions and HPLC-grade water was used for chromatography.

2.2. Chemical reactions

Sodium phosphate buffer (pH 8.0, 100 mM) was prepared by mixing 100 mM aqueous solutions of NaH_2PO_4 and Na_2HPO_4 in a 6.8:93.2 ratio as per Cold Spring Harbor Protocols (Anon., 2006). Reactions were carried out at ambient temperature in 12×32 mm screwcap sample vials (Waters) with the caps containing PTFE/silicone septa to permit direct evaluation by HPLC. GDA (100 μg) was dissolved in MeOH (500 μL) and combined with 500 μL of the phosphate buffer. The sample was maintained at 20–22 °C and analyzed at daily intervals by HPLC. The 1:1 solvent mixture provided solubility for both the GDA and sodium phosphate. HPLC analysis was carried out on a Waters Alliance e2695 separations module equipped with a model 2998 photodiode array detector (PDA) controlled by Waters Empower software. Reactions were analyzed periodically by HPLC using a Phenomenex Luna, 250×4.0 mm, 5 μm C18 column or Waters Bridge C18, 3.5 μm , 4.6×150 mm column. Gradient elution was: solvent A: H_2O , solvent B: MeCN, flow rate: 1.0 mL min^{-1} , initial conditions 70% A, 30% B, going to 1% A, 99% B over 10 min. The effluent was monitored at 200 nm plus a longer wavelength with 254 nm being employed for scouting runs and 222 nm for specific monitoring of GDC, long wavelength tautomers of GDA-sa and other products containing α,β -unsaturated carbonyl chromophores. Molar absorptivity of GDC at 200 nm is about half those of GDA and GDB. The PDA software permitted full UV spectra to be recorded on peaks of interest.

Samples for MS analysis on the total product mixture were collected and evaporated to dryness (Savant SpeedVac). The residue was triturated with CHCl_3 or C_6H_6 . Supernatants were collected, filtered using 3 μm PTFE spin filters and evaporated to dryness in vacuo via SpeedVac. All samples were taken up in MeOH for MS analysis.

2.3. Intracellular and extracellular metabolites from cultures of *A. monilatum* and *pseudogonyaulax*

A culture of *A. monilatum* was established from cells collected via plankton nets in the York River, VA in 2007, and grown in L1 medium without silicate (L1-Si) (Guillard and Hargraves, 1993; Kilham et al., 1998) made with 0.22 μm -filtered natural sea water obtained from Wachapreague, VA at a salinity of 20 ppt. The cultures were grown at 25 °C, in a light: dark cycle of 12 h:12 h at a light intensity of $210 \pm 21 \mu\text{mol photons} \cdot \text{m}^{-2} \cdot \text{s}^{-1}$. Toxin extraction was adapted from Gaillard et al. (2023) for *A. monilatum* cell pellets (intracellular toxins) and Smith et al. (2018) for culture supernatant (extracellular toxins). Briefly, after dilution of culture with fresh medium, a sample was withdrawn and centrifuged (2000 rcf at 4 °C for 10 min) to sediment the cells. The supernatant was then carefully removed. The remaining pellet was extracted with 1.5 mL of MeOH using vortex and bath sonication (25 kHz at < 20 °C for 15 min) and centrifuged (3234 rcf at 4 °C for 10 min) to separate out the cellular debris. The methanolic fraction was filtered through a 0.22 μm PTFE syringe filter (Millipore, Sigma, Burlington, MA, USA), transferred to a glass HPLC vial, evaporated to dryness in vacuo with a Savant SpeedVac and stored at –20 °C until MS analysis. The culture supernatants were extracted using a 60-mg Oasis HLB solid phase extraction (SPE) cartridge (Waters Inc., Milford, MA, USA). Goniodomins were eluted with MeOH, transferred to a glass HPLC vial, evaporated to dryness in vacuo (Savant SpeedVac) and stored at –20 °C until LC-MS analysis.

A culture was prepared from *A. pseudogonyaulax* (isolate X-LF-12-D1) obtained from Limfjord. The supernatant (250 mL, cell density 1278 cells $\cdot \text{mL}^{-1}$) was stored at –20 °C for almost five months prior to processing. The supernatant was concentrated using a C18 SPE cartridge (Supelco) which had been conditioned with 2 mL MeOH and equilibrated with 2 mL deionized H_2O prior to sample application. After application of the supernatant, the cartridge was washed with 10 mL deionized H_2O for removal of salts. The retained GDs were eluted with MeOH in five fractions of 5 mL each. The fractions were collected and concentrated to a final volume of 250 μL each in a rotary evaporator (Heidolph Instruments, Schwabach, Germany). The fraction that eluted first was centrifuged through a spin filter to remove macromolecules and then transferred to an HPLC vial for analysis.

2.4. Analysis of intra- and extracellular GDs formed by *A. pseudogonyaulax* in coastal waters of northern Denmark

2.4.1. Intracellular GDs; net haul extracts of GDs

Samples taken during an oceanographic expedition with R/V Uthörn

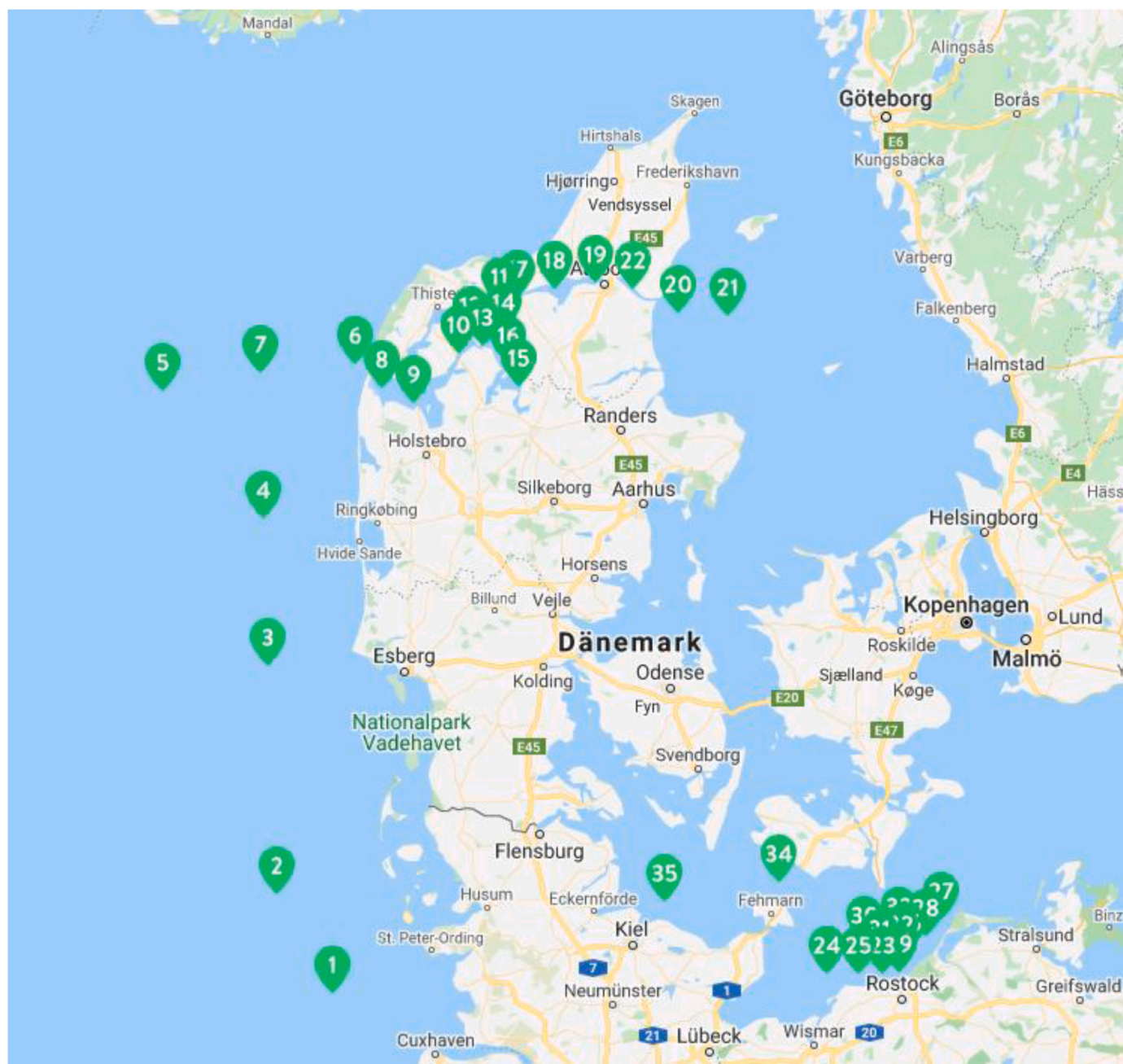


Fig. 1. Sampling stations employed for the 2020 field survey in coastal Denmark. Stations 8–19 and 22 lie in Limfjord and were the primary location of GDA. (Map created with Itilog).

in fall 2020 were collected along the German West coast, the Danish Limfjord strait and the Western Baltic Sea (Fig. 1). Vertical net hauls were employed with 20 μm mesh phytoplankton net (Model 438,030, HYDRO-BIOS, Kiel, Germany). Plankton concentrates were filtered through a three-stage gauze filter with mesh sizes 200, 50 and 20 μm . Material from each mesh was transferred to conical tubes in small volumes of filtered seawater and was pelleted by centrifugation. The supernatants were removed and the cell pellets were stored at $-20\text{ }^{\circ}\text{C}$ until extraction. A portion of the cell pellets was extracted on board the research vessel; the remaining pellets were extracted after return. For extraction, 0.9 g lysing matrix D (ThermoSavant, Illkirch, France) and 1 mL MeOH were added. Cells were homogenized by reciprocal shaking at $6.5\text{ m} \cdot \text{s}^{-1}$ for 45 s (FastPrep-24 5G, MP Biomedicals, Eschwege, Germany) and subsequently centrifuged for 15 min at 16,100 rcf. The resulting supernatants were filtered through spin filters (1 min, 10,000

rcf). Filtrates were immediately transferred to HPLC vials for LC-MS/MS analysis.

2.4.2. GDs extracted from the water column with SPATTs

SPATT (Solid Phase Adsorption Toxin Tracking), bags (MacKenzie et al., 2004) containing 3.0 g of DIAION HP20 (Supelco) polystyrene beads were positioned at the outflow of a ferry box on the expedition vessel and replaced approximately every 96 h. After collection was complete, the SPATT bags were washed with deionized water and dried overnight in a drying oven at $50\text{ }^{\circ}\text{C}$. The resin was transferred from the bags to 50 mL conical tubes. The samples were shaken in 30 mL MeOH overnight. The following day, the methanol was eluted from the resin using chromatography columns. The resin was added to the column and rinsed with 25 mL MeOH. The extract was rotary evaporated to approximately 1 mL, transferred to 1.5 mL Eppendorf tubes and reduced

Table 1

Compound names, screened adducts, and mass transitions for Waters spectrometer.

Compound Name	Adduct	Transition
9-desmethyl GDA	NH ₄ ⁺	772.5 > 593.3
34-desmethyl GDA	NH ₄ ⁺	772.5 > 607.5
GDA, GDB	NH ₄ ⁺	786.5 > 139.5
GDA, GDB	NH ₄ ⁺	786.5 > 607.5
GDA, GDB	Na ⁺	791.5 > 413.3
GDA, GDB	Na ⁺	791.5 > 720.5
GDA, GDB	Na ⁺	791.5 > 747.5
GDC, GDA-sa	NH ₄ ⁺	804.5 > 139.5
GDC, GDA-sa	NH ₄ ⁺	804.5 > 607.5
GDC, GDA-sa	NH ₄ ⁺	804.5 > 751.5
GDC, GDA-sa	Na ⁺	809.5 > 747.5
GDC, GDA-sa	Na ⁺	809.5 > 765.5
GDC-sa	NH ₄ ⁺	822.5 > 113.5
GDC-sa	NH ₄ ⁺	822.5 > 139.5
GDC-sa	NH ₄ ⁺	822.5 > 733.5

to dryness under a nitrogen stream. The dry residue was resuspended in 400 µL MeOH, transferred to a spin filter and centrifuged for 1 min (10,000 rcf). The samples were placed in HPLC vials for LC-MS/MS analysis.

2.5. Mass spectrometry

2.5.1. Bruker 10 T APEX-Qe FT-ICR mass spectrometer (Old Dominion Univ., Norfolk, VA, USA)

The FT-ICR mass spectrometer was employed to acquire the high resolution mass spectra described in Section 3.3. Electrospray ionization was used. The samples were introduced by direct infusion of a MeOH solution using a syringe pump. Sodium adducts were observed using adventitious Na⁺ contained in the samples. Collision-induced dissociation (CID) spectra were acquired using argon as the collision gas. An 8 Da isolation window was employed with the CID voltage optimized. Empirical formulas were assigned using ChemCalc (Patiny and Borel, 2013).

2.5.2. Waters Xevo® TQ-XS mass spectrometer (AWI, Bremerhaven, Germany)

LC-MS/MS samples described in Sections 3.1 and 3.4 were analyzed by ultrahigh-performance liquid chromatography (UPLC) coupled with tandem quadrupole mass spectrometry (LC-MS/MS). The UPLC system consisted of a column oven, an autosampler and a binary pump (ACQUITY I UPLC Class, Waters) and was coupled to a triple quadrupole mass spectrometer (Xevo TQ-XS, Waters). The autosampler was thermostated at 10 °C and sample separation was performed on a RP-18 column (PurospherSTAR endcapped (2 µm) Hibar HR 50–2.1, Merck, Darmstadt, Germany) equipped with a pre-column (0.5 µm, OPTI-SOLV EXP™, Sigma-Aldrich, Hamburg, Germany) held at 40 °C. An alkaline elution system was used for NH₄⁺ adducts with eluent A consisting of 6.7 mM aqueous NH₃ and eluent B 9:1 (v/v) MeCN and 6.7 mM aqueous NH₃. For measurements of sodium adducts an acidic system was used with

Table 2

Mass spectrometric parameters of CID experiments for Waters spectrometer.

Parameter	Setting
Capillary voltage	3 kV
Cone voltage	40 V
Source temperature	150 °C
Desolvation temperature	600 °C
Desolvation gas	1000 L h ⁻¹
Cone gas	150 L h ⁻¹
Nebuliser gas	7.0 bar
Collision gas flow	0.15 mL min ⁻¹
Scan time	0.072 s
Mass range	m/z 100–820

eluent A consisting of 0.2% formic acid and 0.004% aqueous NH₃ and eluent B of 0.2% formic acid and 0.004% aqueous NH₃ in MeCN. The flow rate was 0.6 mL min⁻¹ and initial conditions of 5% B were held for 1.5 min. Then a linear gradient from 5% B to 100% B was performed within 2 min (until 3.5 min) followed by isocratic elution with 100% B for 3 min (until 6.5 min) prior to return to initial conditions within 0.5 min and 1 min equilibration time (total run time: 8 min).

Dwell times, cone voltage and collision energy used in selected reaction monitoring (SRM) experiments in the positive ionization mode were 0.06 s, 40 V, and 40 eV, respectively. The applied mass transitions are listed in Table 1 and the mass spectrometric parameters are given in Table 2. The collision energies for ammonium adducts were 30 eV and for sodium adducts 45 eV. Data were acquired and analyzed with MassLynx (Version 4.2, Waters).

2.5.3. Sciex 4000 QTrap mass spectrometer (IFREMER, Nantes, France)

Analysis of samples was performed on an LC-MS/MS system with a Nexera Ultra-Fast Liquid Chromatography system (UFLC-XR, Shimadzu, France). Separation was achieved on a Xbridge BEH C18 column (50 × 2.1 mm, 2.5 µm) equipped with a pre-column maintained at 40 °C. An alkaline elution gradient was used, started with 2 min at 85% eluent A (water, 6.7 mM NH₄OH) and 15% eluent B (95% ACN, 6.7 mM NH₄OH), followed by a linear increase of B to 100% in 7 min, held for 3 min before going back to initial conditions in 0.5 min and then 2 min equilibration. The flow rate was 0.3 mL min⁻¹, and the injection volume was 5 µL.

The API 4000 QTrap hybrid triple quadrupole ion trap mass spectrometer (Sciex, France) was used in positive electrospray ionization MRM mode and both ammonium (M + NH₄⁺) and sodium (M + Na⁺) adducts were monitored (Table 3). The instrumental parameters were optimized by flow injection analysis using the GDA standard: curtain gas: 25 psi; collision gas: high; ion spray voltage: 5000 V; temperature: 450 °C; nebulizer/auxiliary gas: 40/45 psi.

3. Results

3.1. Stability of GDA

Studies of the stability of GDA in anhydrous MeOH, deionized water, and pH 8.0 Keller culture medium (K-medium) (Keller et al., 1987) showed that no decomposition occurred in MeOH within 10 days but over that time period more than 90% of the GDA had decomposed in deionized water and it had fully decomposed in pH 8.2 K-medium (Fig. 2). GDA, GDB, GDC, GDA-sa and the seco acid of GDC (GDC-sa), were monitored during the 10-day incubations. In both deionized water and K-medium, the dominant product had a molecular weight 18 Da higher than GDA and was provisionally identified as GDA-sa. GDA-sa

Table 3

Compound names, screened adducts, and mass transitions for API spectrometer.

Compound Name	Adduct	Transition
34-desmethyl GDA	NH ₄ ⁺	772.5 > 125.4
34-desmethyl GDA	NH ₄ ⁺	772.5 > 607.5
34-desmethyl GDA	NH ₄ ⁺	772.5 > 719.5
GDA, GDB	NH ₄ ⁺	786.5 > 139.0
GDA, GDB	NH ₄ ⁺	786.5 > 607.2
GDA, GDB	NH ₄ ⁺	786.5 > 733.4
GDC, GDA-sa	NH ₄ ⁺	804.5 > 139.5
GDC, GDA-sa	NH ₄ ⁺	804.5 > 607.5
GDC, GDA-sa	NH ₄ ⁺	804.5 > 751.5
GDC-sa	NH ₄ ⁺	822.5 > 139.5
GDC-sa	NH ₄ ⁺	822.5 > 733.5
GDA, GDB	Na ⁺	791.4 > 413.2
GDA, GDB	Na ⁺	791.4 > 747.3
GDA, GDB	Na ⁺	791.4 > 765.3
GDC, GDA-sa	Na ⁺	809.5 > 747.5
GDC, GDA-sa	Na ⁺	809.5 > 765.5
GDA-sa	2Na ⁺	831.4 > 423.1

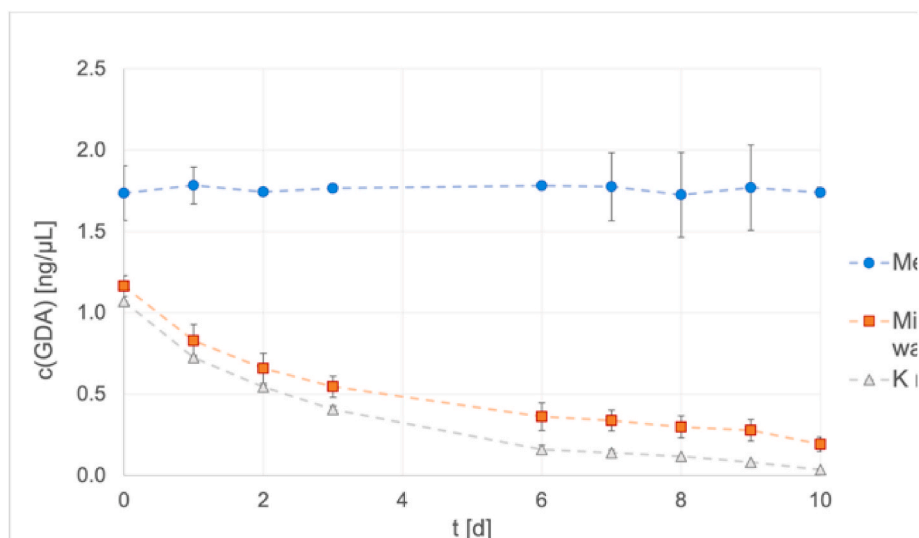


Fig. 2. Time course of the disappearance of GDA in MeOH, deionized water and K-medium. Error bars represent standard deviations of three measurements.

and GDC are isomeric but differ in HPLC retention times. Both can be observed with SRM transitions of m/z 804.5 > 751.5 and 804.5 > 139.5 for NH_4^+ adducts. A small amount (<1%) of a compound having molecular weight 36 Da higher than GDA and SRM transitions of m/z 822.5 > 733.5 and 822.5 > 139.5 was observed and is provisionally assigned as the seco acid of GDC.

3.2. LC-MS/MS behavior of GDA-sa

Mass spectra acquired using solutions in MeOH yielded adducts with adventitious Na^+ . The empirical formula for the resulting GDA-sa (4) was assigned as $\text{C}_{43}\text{H}_{62}\text{O}_{13}$ by accurate mass measurement, i.e., m/z 809.4086 for $\text{C}_{43}\text{H}_{62}\text{NaO}_{13}^+$ and m/z 831.3904 for $\text{C}_{43}\text{H}_{61}\text{Na}_2\text{O}_{13}^+$ (Table 4). The formula indicates that the transformation involved the addition of one molecule of water. The MS spectrum of the crude product mixture showed the presence of small quantities (~10%) of methanolysis products, reflecting competition between water and MeOH in the ring-opening process.

A high-resolution CID (collision-induced dissociation) spectrum was acquired on the m/z 831.3902 disodio adduct of GDA-sa. These data are presented in Table 5. Overall, 33 fragment ions were observed for which empirical formulas could be assigned. For 25 of them, the specific

carbon atoms comprising the fragment could also be assigned with reasonable certainty. These fragment ions fall into four classes: three disodiated and three monosodiated head fragments having the carboxyl group still attached, 10 monosodiated head fragments that had lost the carboxyl group and nine monosodiated tail fragments. Satisfactory carbon assignments could not be made for 8 of the fragment ions. These were not intense signals. They may be internal in the chain, arising by nicking at two locations, but alternatively they may be artifacts. Overall, the CID data support structures 4a and 4b for GDA-sa by showing cleavage occurring at the following C–C bonds: C1–C2, C10–C11, C12–C13, C13–C14, C18–C19, C22–C23, C26–C27 and C27–C28.

Chromatographic data acquired on a UPLC-linked triple quadrupole electrospray mass spectrometer revealed partial resolution of isomers of GDA-sa. Na^+ and NH_4^+ adducts are displayed in Fig. 3a and b, respectively. GDA-sa partitioned into multiple peaks. For the Na^+ adducts, the fast-running peak was broadened and had a ragged shape, indicative of structural heterogeneity. The slower running peak was sharper but had a small, broad peak following it. The two peaks were treated as a single one. The NH_4^+ peaks were sharper than the Na^+ and deceptively appeared to be more homogeneous. The third peak was not observed in the NH_4^+ chromatogram, presumably due to it coeluting with peak 2. With both the Na^+ and NH_4^+ adducts, the fast-eluting peak was the largest.

CID of Na^+ adducts of the fast-running chromatographic peak gave fragment ions (Fig. 3a and Table 6) that were essentially the same as those that had been observed with the FT-ICR spectrometer. This is not unexpected since the FT-ICR data had been acquired with unfractionated products and are the sum of concentration-weighted fragmentation data for the two chromatographic peaks observed with the LC-MS/MS. Furthermore, the differences in fragmentation spectra between the two fractions were small. The high-resolution data obtained with the FT-ICR spectrometer aided in assignment of empirical formulas of fragments observed with the LC-MS/MS instrument.

CID spectra of the NH_4^+ adducts were acquired for both chromatographic peaks. The fragment ions are listed in Table 7. Loss of NH_3 occurred first, followed by five successive losses of water molecules. In the fast-running (2.20 min) peak (Fig. 3b), the m/z 733.1 ion, resulting from loss of NH_3 plus three water molecules, is the most intense fragment ion in the spectrum. Intense fragment ions are also observed in the low mass region at m/z 223.5, 147.3, 139.3, 121.3 and 113.5. The m/z 139.3, 121.3 and 113.5 signals are provisionally assigned as $\text{C}_9\text{H}_{15}\text{O}^+$, $\text{C}_9\text{H}_{13}\text{O}^+$ and $\text{C}_7\text{H}_{13}\text{O}^+$, respectively. Their location in the molecule, i.e., ring A or ring F, is still under investigation. Reliability of less intense

Table 4

Hydrolysis and methanolysis products of GDA. Mono and disodio adducts of the products of hydrolysis (a) and methanolysis (b) from the reaction of GDA with pH 8.0 sodium phosphate buffer in 1:1 (v:v) MeOH– H_2O . The spectrum was acquired using an FT-ICR mass spectrometer with direct infusion of a methanolic solution of the crude product after desalting by extraction into benzene.

(a) Hydrolysis product (GDA-sa, $\text{C}_{43}\text{H}_{62}\text{O}_{13}$)						
Obs (m/z)	Intensity	Formula	Calcd (m/z)	Δ (ppm)	Assignment	
809.4086	5.3e7	$\text{C}_{43}\text{H}_{62}\text{NaO}_{13}^+$	809.4083	0.42	GDA-sa + Na^+	
831.3904	5.8e7	$\text{C}_{43}\text{H}_{61}\text{Na}_2\text{O}_{13}^+$	831.3902	0.23	GDA-sa - H^+ + 2Na^+	
Σ 1.1e8						
(b) Methanolysis product (Me-GDA-sa, $\text{C}_{44}\text{H}_{64}\text{O}_{13}$)						
Obs (m/z)	Intensity	Formula	Calcd (m/z)	Δ (ppm)	Assignment	
823.4243	4.9e6	$\text{C}_{44}\text{H}_{64}\text{NaO}_{13}^+$	823.4239	0.47	Me-GDA-sa + Na^+	
845.4067	5.8e6	$\text{C}_{44}\text{H}_{63}\text{Na}_2\text{O}_{13}^+$	845.4059	1.00	Me-GDA-sa - H^+ + 2Na^+	
Σ 1.1e7						

Table 5

Empirical formulas and carbon atom assignments of fragment ions produced by CID of disodio GDA-sa ($C_{43}H_{61}Na_2O_{13}^+$, m/z 831.3886).

a) Disodio C1-CXX fragment ions					
Obs (m/z)	Int.	Formula	Calcd (m/z)	Δ (ppm)	Assignment
813.3786	1.9e6	$C_{43}H_{59}Na_2O_{12}^+$	813.3796	-1.28	C1-C36
423.1384	4.2e6	$C_{20}H_{25}Na_2O_7^+$	423.1390	-1.46	C1-C16
351.1174	1.2e6	$C_{17}H_{21}Na_2O_5^+$	351.1179	-1.39	C1-C13
b) Monosodio C1-CXX fragment ions					
Obs (m/z)	Int.	Formula	Calcd (m/z)	Δ (ppm)	Assignment
791.3957	5.0e5	$C_{43}H_{60}NaO_{12}^+$	791.3953	-2.52	C1-C36
773.3859	5.8e5	$C_{43}H_{58}NaO_{11}^+$	773.3871	-1.59	C1-C36
401.1565	4.3e6	$C_{20}H_{26}NaO_7^+$	401.1571	-1.43	C1-C16
c) Monosodio C2-CXX fragment ions					
Obs (m/z)	Int.	Formula	Calcd (m/z)	Δ (ppm)	Assignment
765.4172	1.8e6	$C_{42}H_{62}NaO_{11}^+$	765.4184	-1.61	C2-C36
747.4065	2.0e6	$C_{42}H_{60}NaO_{10}^+$	747.4079	-1.83	C2-C36
729.3961	1.2e6	$C_{42}H_{58}NaO_9^+$	729.3973	-1.65	C2-C36
565.2763	1.8e6	$C_{31}H_{42}NaO_8^+$	565.2772	-1.57	C2-C27
467.2397	7.2e5	$C_{26}H_{36}NaO_6^+$	467.2404	-1.52	C2-C27
357.1667	1.9e7	$C_{19}H_{26}NaO_5^+$	357.1672	-1.52	C2-C16
349.1769	1.9e7	$C_{21}H_{26}NaO_5^+$	349.1774	-1.48	C2-C18
287.1250	3.6e6	$C_{15}H_{20}NaO_4^+$	287.1254	-1.32	C2-C12
233.1145 ¹	1.0e6	$C_{12}H_{18}NaO_3^+$	233.1148	-1.35	C2-C10
231.0989	1.5e6	$C_{12}H_{16}NaO_3^+$	231.0992	-1.15	C2-C10
d) Monosodio CYY-C36 fragment ions					
Obs (m/z)	Int.	Formula	Calcd (m/z)	Δ (ppm)	Assignment
537.2814	6.0e5	$C_{30}H_{42}NaO_7^+$	537.2823	-1.63	C11-C36
495.2345 ¹	1.2e6	$C_{27}H_{36}NaO_7^+$	495.2353	-1.66	C13-C36
431.2398	1.8e7	$C_{23}H_{36}NaO_6^+$	431.2404	-1.41	C17-C36
429.2241 ¹	1.6e6	$C_{23}H_{34}NaO_6^+$	429.2248	-1.54	C17-C36
413.2292	3.5e7	$C_{23}H_{32}NaO_6^+$	413.2298	-1.56	C17-C36
395.2187	2.6e7	$C_{23}H_{32}NaO_4^+$	395.2193	-1.47	C17-C36
377.2082	2.2e6	$C_{23}H_{30}NaO_3^+$	377.2087	-1.37	C17-C36
367.1875 ¹	1.8e6	$C_{21}H_{28}NaO_4^+$	367.1880	-1.31	C19-C36
251.1251	5.1e5	$C_{12}H_{20}NaO_4^+$	251.1254	-1.11	C27-C36
e) Monosodio CYY-CXX fragment ions					
Obs (m/z)	Int.	Formula	Calcd (m/z)	Δ (ppm)	Assignment
603.1772	5.5e5	$C_{38}H_{28}NaO_6^+$	603.1778	-1.01	Not assigned
565.1022	4.8e5	$C_{35}H_{19}Na_2O_5^+$	565.1022	-0.07	Not assigned
425.2868	5.5e5	$C_{22}H_{42}NaO_6^+$	425.2874	-1.32	Not assigned
423.1356	9.8e5	$C_{29}H_{20}NaO_7^+$	423.1356	0.12	Not assigned
415.1721	3.8e6	$C_{21}H_{28}NaO_7^+$	415.1727	-1.50	Not assigned
413.2265	7.6e5	$C_{21}H_{35}Na_2O_5^+$	413.2264	0.30	Not assigned
385.1980	3.3e6	$C_{21}H_{30}NaO_5^+$	385.1985	-1.41	Not assigned
255.0601	6.4e5	$C_{11}H_{13}Na_2O_4^+$	255.0604	-1.07	Not assigned

¹Ions unique to the FT-ICR instrument.

ions in the NH_4^+ data is undercut by nonspecific chemical decomposition in the ion source which creates artifactual signals at odd-numbered m/z values. The intensities of these artifacts are highest between m/z 100 and 300. In many cases they made it impossible to distinguish the weaker mechanism-based fragment signals from strong artifacts, limiting the effective dynamic range of the CID spectra of NH_4^+ adducts. Substantial differences in fragment ion intensities between the fast- and slow-running chromatographic peaks are indicated with red arrows in Fig. 4b and c.

3.3. Intracellular and extracellular GDs formed by laboratory cultures

The facile non-enzymatic cleavage of GDA to form GDA-sa impacts the distribution of the two compounds between cells and growth medium in laboratory cultures (See Section 2.3). The intracellular and extracellular extracts were analyzed for GDA, GDA-sa, GDB and GDC by LC-MS/MS. Fig. 5 shows that the intracellular GDA concentration was far greater than that of GDA-sa while the extracellular concentration of

GDA-sa was far greater than that of GDA. In both situations the amounts of GDB and GDC were negligible. Similar observations have been made with cultures of *A. hiranoi*, *A. pseudogonyaulax* and *A. taylorii* (Hintze, 2021).

3.4. Analysis of intra- and extracellular goniodomains formed by *A. pseudogonyaulax* in Limfjord and coastal waters of northern Denmark

The fall 2020 oceanographic expedition extended from the German west coast through the Danish Limfjord strait into the Kattegat and the Western Baltic Sea covering German coastal waters (Fig. 1). In an examination of the algal constituents of the field samples, *A. pseudogonyaulax* was found at almost all stations but highest cell densities were observed in Limfjord (U. Tillmann, unpublished data). MS analyses showed GDA to be present in the cell extracts from plankton concentrates of samples collected at all sampling sites with the highest concentrations being in Limfjord. GDA-sa had not been monitored in the earlier survey. The 2020 survey broadened the analyses to include GDA, GDB, GDC, GDA-sa and GDC-sa. The LC-MS analyses were carried out under four sets of conditions comprising acidic and basic HPLC eluents with MS analysis being carried out with NH_4^+ and Na^+ adducts (Fig. 6).

MS analysis of extracts of a pair of HP20 SPATTs that had been exposed to seawater in the Limfjord via the ship's ferrybox (see Section 2.4.1) showed that GDA-sa was present ($0.13 \text{ ng} \cdot \mu\text{L}^{-1}$) whereas GDA, if present at all, was below the level of detection. Interestingly, GDC-sa was also present at levels comparable to GDA-sa. Adjacent areas of the German bight and Kattegat gave similar results. Unexpectedly, a site in the western Baltic Sea contained high levels of GDA-sa and GDC-sa (3.48 and $1.48 \text{ ng} \cdot \mu\text{L}^{-1}$, respectively); GDA was also present ($0.10 \text{ ng} \cdot \mu\text{L}^{-1}$). That site deserves further investigation on future expeditions. To summarize the changes in Sections 3.3 and 3.4, I have compiled a revised version of these two sections and sent a copy to Mr. Vijay Kuppasami. (Fig. 7)

4. Discussion

4.1. Stability of GDA

The stability of GDA was reinvestigated due to inconsistencies in earlier reports (Onofrio, 2020; Hintze, 2021). The stability in pure water was particularly problematic because the pH of pure water, including that collected from the Milli-Q water purifier, cannot be measured reliably due to low conductivity. Crystalline GDA has been found to have excellent stability at room temperature although as a safety precaution it has normally been stored at -20°C . The stability in aprotic solvents and in anhydrous MeOH and *d*₄-MeOH appears to be good. Takeda et al. (2008) employed $CDCl_3$, $C_6H_6-d_6$, acetone-*d*₆, CD_2Cl_2 and *d*₄-MeOH for NMR studies with no evidence of degradation. Nevertheless, we have observed that care has to be taken to maintain rigorously anhydrous conditions when working with solutions in acetone and MeOH because moisture acquired during storage and thermal cycling will lead to gradual degradation. Overall, there is a sharp distinction between the stability of GDA in MeOH and instability in water.

4.2. Parent ions of products of GDA ring cleavage

The primary product of ring-opening by H_2O is GDA-sa (4) or, more strictly speaking, stereoisomers and tautomers of 4. The presence of the carboxylic acid group is indicated by observation of a disodio adduct ($C_{43}H_{61}Na_2O_{13}^+$; m/z 831.3886; $GDA + H_2O + 2Na^+ - H^+$), which is a signature for analytes being carboxylic acids (Murphy, 2014). GDA-sa is isomeric to GDC (3). Nevertheless, they are readily distinguished by pH dependence of the chromatographic retention time of GDA-sa. The increased polarity of the sodium salt of 4 is demonstrated by it eluting faster than GDC from reverse-phase HPLC columns in aqueous acetonitrile eluents.

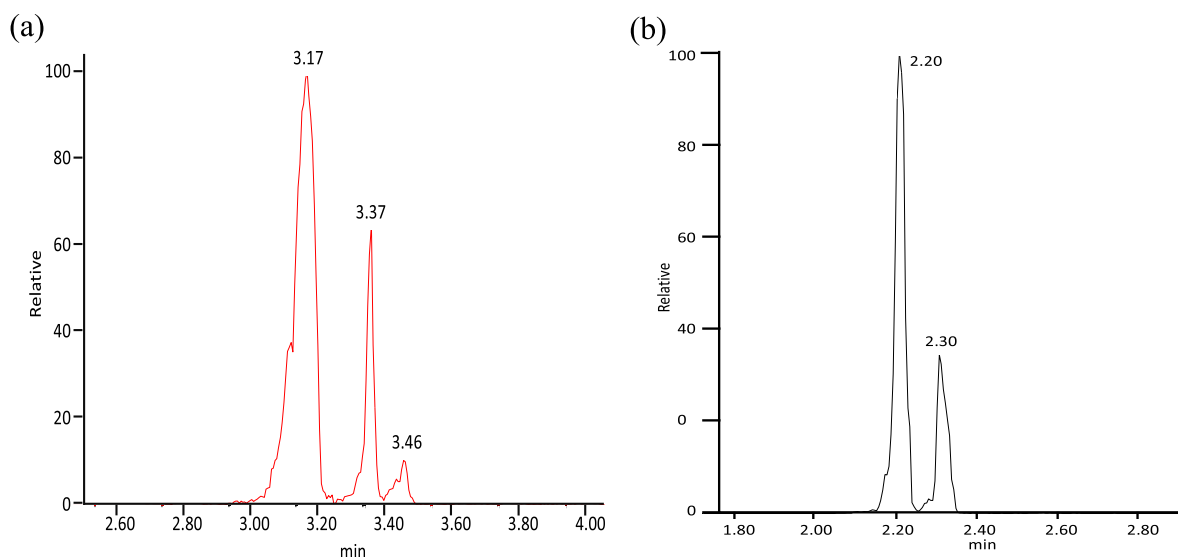


Fig. 3. Chromatographic traces of GDA-sa formed by treatment of GDA with Na phosphate, pH 8.0 in 1:1 MeOH–H₂O. The adducts were monitored with a UPLC-linked triple quadrupole electrospray mass spectrometer with a C18 chromatograph column. (a, left) Na⁺ adducts were separated with Na⁺-optimized eluent and monitored with the m/z 809 > 765 transition. (b, right) NH₄⁺ adducts were separated with NH₄⁺-optimized eluent and monitored with the m/z 804 > 139 transition.

The hydrolysis reaction was carried out in 1:1 (v:v) MeOH–H₂O to create simultaneous solubility of GDA and phosphate buffer. The pH 8 reaction yielded ~10% of methanolysis products formed by competing reactions with MeOH. The disodio adduct observed for the methanolysis products indicated that they had been formed, at least in part, by alkyl-O cleavage of the ester linkage. It should be noted, however, that this does not address the question of whether hydrolysis of GDA occurs by alkyl-O or acyl-O cleavage.

A minor product having a molecular weight 36 Da higher than GDA and SRM transitions of m/z 822.5 > 733.5 and 822.5 > 139.5 was observed and is provisionally assigned as the seco acid of GDC. Its formation was unexpected. We hypothesize that the lactone moiety of GDC is more prone to hydrolysis than that of GDA.

4.3. CID fragmentation of GDA-sa

CID fragmentations play a central role in this paper. Fragmentation of NH₄⁺ adducts of GDA-sa follows pathways that are different from those observed with Na⁺ adducts, so there is merit in acquiring both types of

spectra when carrying out structural studies. There is also merit in examining both FT-ICR and LC-MS/MS spectra. In the present case, high-resolution spectra acquired by FT-ICR revealed doublets, i.e., two ions having the same nominal mass, at m/z 565 (m/z 565.2763 and 565.1022) and at m/z 413 (m/z 413.2292 and 413.2269) (Table 5). These are not resolved with the lower resolution of the triple quadrupole instrument. This leads to ambiguity as to whether one or both signals are present. Albeit, in the case of the m/z 413 ions one of them is of low intensity and has questionable validity. Nevertheless, one should exercise caution using them for structural assignments with the triple quadrupole instrument. Even with the high resolution provided by the FT-ICR spectrometer, doublets may overlap sufficiently that the accuracy of mass measurement will be degraded (Lopes et al., 2002a,b).

The FT-ICR CID spectrum of GDA-sa was acquired for the disodio adduct of GDA-sa while the spectrum acquired with the triple quadrupole instrument was that of the monosodio adduct. Nevertheless, there is good correspondence between the two although the triple quadrupole CID spectrum contained ions at m/z 609.1 and 695.1 that were not present in the FT-ICR spectrum. The rather weak m/z 609.1 ion is tentatively assigned as the C1–C27 head fragment (C₃₂H₄₂NaO₁₀⁺) and

Table 6

CID spectrum of the Na⁺ adducts of GDA-sa (m/z 809).

m/z	3.17 min	3.37 min	Formula	Assignment
	Rel. Int. (%)	Rel. Int. (%)		
791.2	14	8	C ₄₃ H ₆₀ NaO ₁₂ ⁺	C1–C36
773.3	7	–	C ₄₃ H ₅₈ NaO ₁₀ ⁺	C1–C36
765.2	100	100	C ₄₂ H ₆₂ NaO ₁₁ ⁺	C2–C36
747.1	23	14	C ₄₂ H ₆₀ NaO ₁₀ ⁺	C2–C36
729.3	10	2	C ₄₂ H ₅₈ NaO ₉ ⁺	C2–C36
695.1 ^a	8	8	C ₃₈ H ₅₆ NaO ₁₀ ⁺	C5–C36
613.0	–	4	Not assigned	
609.1 ^a	4	–	C ₃₂ H ₄₂ NaO ₁₀ ⁺	C1–C27
565.2	12	–	C ₃₁ H ₄₂ NaO ₉ ⁺	C2–C27
537.2	4	3	C ₃₀ H ₄₂ NaO ₇ ⁺	C2–C26
431.1	84	68	C ₂₃ H ₃₆ NaO ₆ ⁺	C17–C36
413.3	27	13	C ₂₃ H ₃₄ NaO ₅ ⁺	C17–C36
401.0	18	20	C ₂₀ H ₂₆ NaO ₇ ⁺	C2–C16
395.2	8	–	C ₂₃ H ₃₂ NaO ₄ ⁺	C17–C36
357.2	24	25	C ₁₉ H ₂₆ NaO ₅ ⁺	C2–C16
287.2	4	5	C ₁₂ H ₂₀ NaO ₄ ⁺	C25–C36
251.1	4	2	C ₁₂ H ₂₀ NaO ₄ ⁺	C27–C36
231.3	6	–	C ₁₂ H ₁₆ NaO ₃ ⁺	C2–C10

^a The m/z 695.1 and 609.1 ions are unique to the LC-MS/MS instrument.

Table 7

CID spectr of the GDA-sa, NH₄⁺ adduct (m/z 804).

m/z	2.20 min	2.30 min	Formula	Assignment
	Rel. Int (%)	Rel. Int (%)		
769.0	8	3	C ₄₃ H ₆₁ O ₁₂ ⁺	C1–C36
751.1	51	53	C ₄₃ H ₅₉ O ₁₁ ⁺	C1–C36
733.1	100	100	C ₄₃ H ₅₇ O ₁₀ ⁺	C1–C36
715.1	60	56	C ₄₃ H ₅₅ O ₉ ⁺	C1–C36
697.1	20	20	C ₄₃ H ₅₅ O ₉ ⁺	C1–C36
607.1	11	5	C ₃₅ H ₄₃ O ₉ ⁺	C1–C30
579.1	–	16	Not assigned.	
565.1	13	18	Not assigned	
547.2	14	13	Not assigned	
528.9	10	13	Not assigned	
275.4	26	36	Not assigned	
223.5	30	62	Not assigned	
209.4	<5	51	Not assigned	
177.5	<5	32	Not assigned	
147.3	42	26	Not assigned	
139.3	43	37	C ₉ H ₁₅ O ⁺	Not assigned
121.3	30	41	C ₉ H ₁₃ ⁺	Not assigned
113.5	79	–	C ₇ H ₁₃ O ⁺	Not assigned

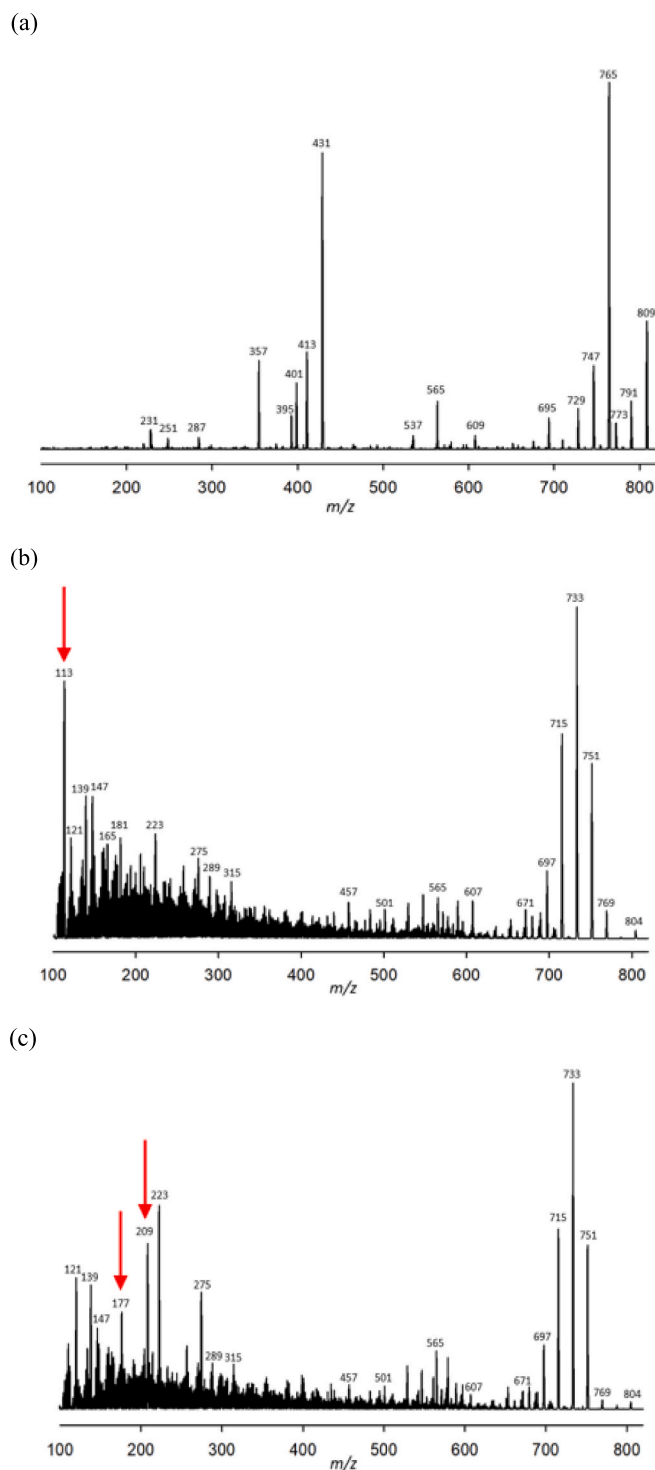


Fig. 4. CID spectra of Na⁺ and NH₄⁺ adducts of GDA-sa. (a) Na⁺ adduct (m/z 809) of the fast-running 3.17-min peak of GDA-sa ($C_{43}H_{62}NaO_{13}^+$, m/z 809). The m/z 695.1 and 609.1 ions are unique to the Waters instrument and are underlined in Table 6. Fragment ions of NH₄⁺ adducts (m/z 804) of the fast- and slow-running 2.20- and 2.30-min peaks, respectively, of GDA-sa. In panels b and c, substantial differences in fragment ion intensities between the fast- and slow-running chromatographic peaks are indicated with red arrows in Fig. 4b and c. (For interpretation of the references to colour in this figure legend, the reader is referred to the Web version of this article.)

the somewhat stronger m/z 695.1 ion as the C5–C36 tail fragment ($C_{38}H_{56}NaO_{10}^+$). The FT-ICR CID spectrum contained four monosodio fragment ions (m/z 495.2345, 429.2241, 367.1875 and 233.1145) that were not observed in the triple quadrupole spectrum. These are underlined in Table 5. Based on their accurate masses, the empirical formulas of the unique peaks can be assigned as $C_{27}H_{36}NaO_7^+$, $C_{23}H_{34}NaO_6^+$,

$C_{21}H_{28}NaO_4^+$ and $C_{12}H_{18}NaO_3^+$ and the carbon atom constitutions can be provisionally assigned as C13–C36, C17–C36, C19–C36 and C2–C10. We were unable to make carbon assignments for eight fragment ions observed in the FT-ICR spectrum. Only two (m/z 565.1022 and 413.2265) may actually be present in the triple quadrupole spectrum. Their existence is uncertain because the FT-ICR spectrum revealed that

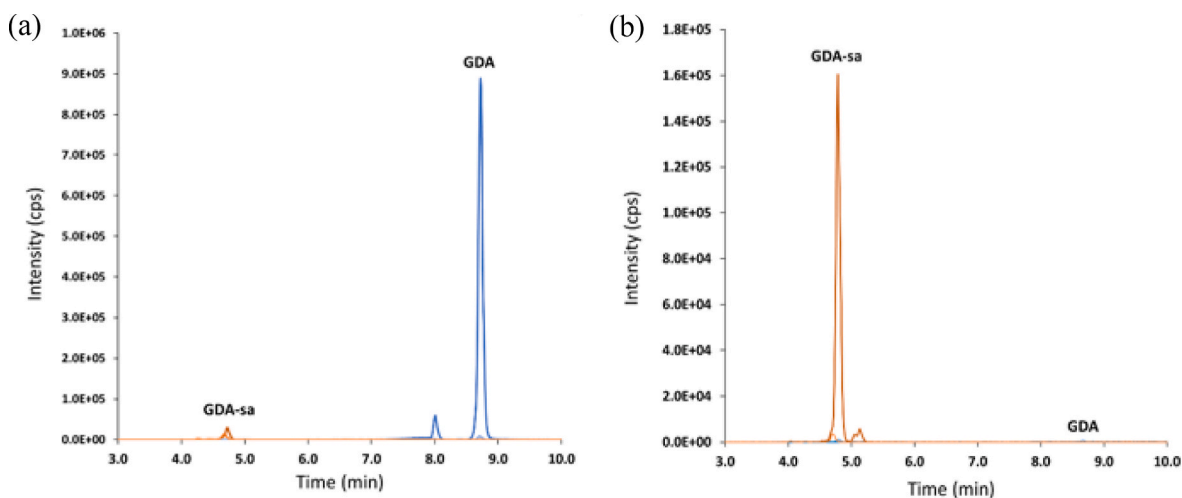


Fig. 5. (a, left) *A. monilatum* cell pellet extract. (b, right) *A. monilatum* supernatant extract. Data acquisition employed summation of transitions for Na^+ and NH_4^+ to compensate for differential ionization efficiencies of GDA and GDA-sa. Note differences in intensity scales for the two plots.

In the supernatant of an *A. pseudogonyaulax* culture established from a sample collected during the Limfjord expedition (isolate X-LF-12-D1), GDA-sa was determined to be the main component with an abundance corresponding to a hypothetical cell quota of $2.58 \text{ pg cell}^{-1}$ (Fig. 6, NH_4^+ adduct, GDA equivalent). GDA-sa accounted for the major proportion of the goniodomins in the culture supernatant, followed by $\sim 10\%$ each of GDA and GDC-sa. The amount of extracellular GDA was $0.26 \text{ pg cell}^{-1}$. GDB and GDC were not detected.

both are paired with peaks having the same nominal masses. Overall, comparison of CID spectra obtained with the two instruments reveals them to have complementary value, strengthening the structural assignment for GDA-sa.

The m/z 423.1386 and 431.2398 fragment ions in the FT-ICR CID spectrum of the sodium adducts of **4a** and **4b** play a major role in establishing the structure of GDA-sa. These ions are formed by a pair of retro-Diels-Alder fragmentations occurring in dihydropyran ring D to create positively charged C1–C16 ene head (m/z 423.1386; $\text{C}_{20}\text{H}_{25}\text{Na}_2\text{O}_7^+$) and C17–C36 diene tail (m/z 431.2398, $\text{C}_{23}\text{H}_{36}\text{NaO}_6^+$) fragments. [Scheme 1](#) illustrates the fragmentations of **4b**. Confirmation of the m/z 431.2398 assignment was obtained from ions at m/z 413.2292 and 395.2187 reflecting sequential losses of two water molecules. Confirmation of the m/z 423.1384 disodio adduct was obtained from a monosodio adduct observed at m/z 401.1565. The triple quadrupole spectrum gave m/z 401.0 and m/z 431.1 head and tail ions. An m/z 413.3 ion, which is likely to be loss of H_2O from m/z 431.1, was also observed but the assignment is ambiguous due to peak pairing.

During separation of the two fragments of the parent cation in the CID process, the fragment that retains the positive charge will be the only one observed. In the present case, two fragmentation processes are occurring concurrently, one creating the charged head fragment and the other the charged tail. Retro-Diels-Alder processes, first reported in mass spectra by [Biemann \(1962\)](#), have been the subject of intensive investigation ([Tureček and Hanuš, 1984](#); [Rickborn, 1998a,b](#)) and have become a powerful tool for structure assignments of acyclic molecules such as GDA-sa.

4.4. Structural and mechanistic considerations in formation of GDA-sa

The reaction of GDA carried out in 1:1 (v/v) MeOH and H_2O created a mixture of hydrolysis and methanolysis products (Na^+ adducts; [Table 4](#)). With methanolysis, acyl-O cleavage would give the seco ester (Path a in the upper section of [Scheme 2](#)). Alkyl-O cleavage would yield seco acids where direct attack by MeOH (Path b) would give the C31 methoxy derivative while allylic attack would give the C29 derivative (Path c). Observation of the disodio adducts of the methanolysis product ([Table 5b](#)) indicated that methanolysis occurred, at least in part, by alkyl-O cleavage, thereby giving carboxylic acids. With hydrolysis, both acyl-O and alkyl-O cleavage would give GDA-sa-1 (Paths d and e in the lower section of [Scheme 2](#)). Alkyl-O cleavage by allylic attack at C29

would give GDA-sa-2 (Path f).

Seco acids might be formed by a more convoluted route involving intramolecular attack of the hemiketal hydroxy group on C31 to form oxirane **5** ([Scheme 3](#)). Hydrolysis of the oxirane could occur by cleavage of the C32–O bond to give **4a** with the incoming hydroxy group being inserted at C32 (Path i). Alternatively, hydrolytic cleavage of the C31–O bond of **5** would give **4a** in which the incoming hydroxy group is at C31 (Path h). Allylic attack on **5** would yield **4b** with the hydroxy group at C29 (Path g). At this point we have no evidence for existence of an oxirane intermediate but it might be an undetected intermediate on the pathway to GDA-sa-1. We hypothesize that under the pH 8 reaction conditions a combination of allylic attack at C29 by Path f ([Scheme 2](#)) and oxirane-mediated Path i ([Scheme 3](#)) is occurring. The products of the two pathways differ. The allylic attack places the incoming hydroxy group at C29 yielding GDA-sa-2 (**4b**) while the oxirane pathway places the hydroxy group at C32 yielding GDA-sa-1 (**4a**). Evidence for the existence of concurrent hydrolytic pathways lies in the two chromatographic peaks, where substantial differences exist between the fragmentations of their NH_4^+ adducts ([Table 7](#)). In particular, the strong signal at m/z 113 is only present in the fast-eluting component.

DFT calculations by [Hess and Smentek \(2022\)](#) led to similar conclusions concerning involvement of dual pathways although they did not give consideration to GDA-sa-2 being a product. Further experimental studies may shed light on this complex problem. Trapping experiments might provide evidence for the involvement of the oxirane, even if it is too unstable to be isolated. Success in characterization of unstable epoxides has occurred in other cases, such as with leukotriene A_4 ([Borgeat and Samuelsson, 1979](#)) and the epoxide of aflatoxin B_1 ([Guengerich et al., 1998](#)).

We conclude that allylic displacement at C29 leading to GDA-sa-2 (**4b**), formed by Path f in [Scheme 2](#) is favored over direct attack at C31 to form GDA-sa-1 (**4a**, formed by Path e in [Scheme 2](#)) due to better access of nucleophiles to C29. The resulting C32-hydroxy group would make **4b** more polar than **4a** where the vicinal C31–C32-hydroxy groups are able to form intramolecular hydrogen bonds. Intramolecular hydrogen bonding would be precluded for stereoisomers of **4b** having *E* configuration for the C30–C31 double bond and disfavored for the *Z* configuration where the hydrogen bond would produce a 7-membered ring. Assignment of **4b** being present in the large, fast-eluting chromatographic peak and **4a** in the smaller, slow-eluting peak **4a** is consistent with **4a** being more lipophilic due to the hydrogen bonding.

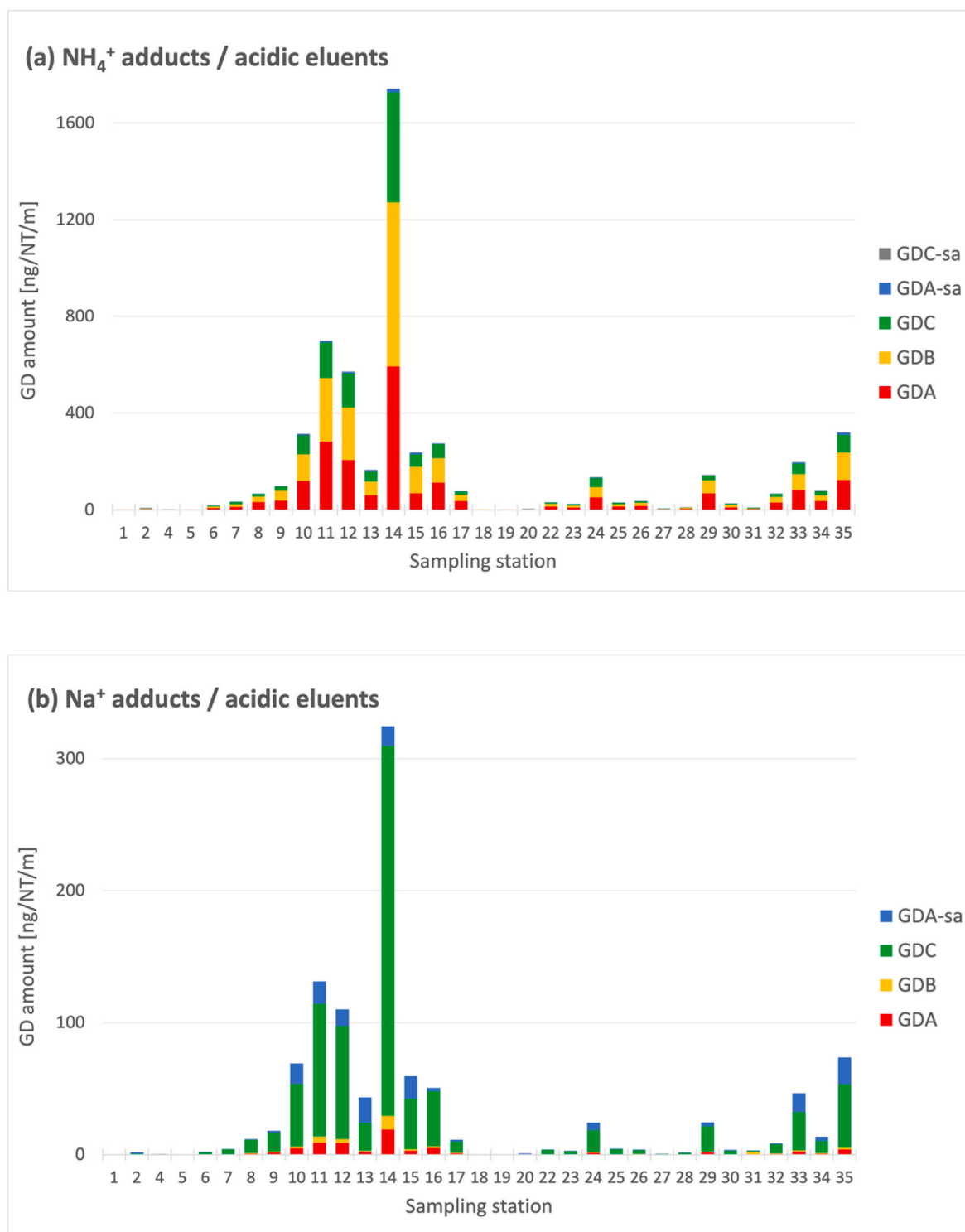


Fig. 6. Intracellular content of GDs. LC-MS analyses of NH₄⁺ and Na⁺ adducts of net haul extracts from plankton concentrates collected from the stations shown in Fig. 1. Acidic eluent was used in panels a and b and basic eluent in c and d. NH₄⁺ adducts were observed in panels a and c and Na⁺ adducts in panels b and d. Concentrations of GDA were calibrated with an external reference sample. GDA-sa, GDB and GDC concentrations are expressed as GDA equivalents.

End absorption in the UV spectrum of the initially formed **4a** and **4b** solvolysis products is consistent with the assignments but **4a** and **4b** would both form C29–C33 structural and configurational isomers via enol-keto tautomerism (Scheme 4). Formation of α,β -unsaturated ketones **4e**, **4f** and **4h** is indicated by the time-dependent appearance of a λ_{\max} 222 nm UV absorption band observed during HPLC of aged samples.

Accurate mass measurement permits empirical formulas to be established for CID fragmentation ions arising from GDA and its macrocyclic congeners but using this information to establish structures of fragmentation is difficult because the cyclic compounds require two bonds to be broken to create the fragment ions, greatly increasing the difficulty of making carbon atom assignments. On the other hand, preliminary hydrolysis of the ester linkage followed by CID studies on the

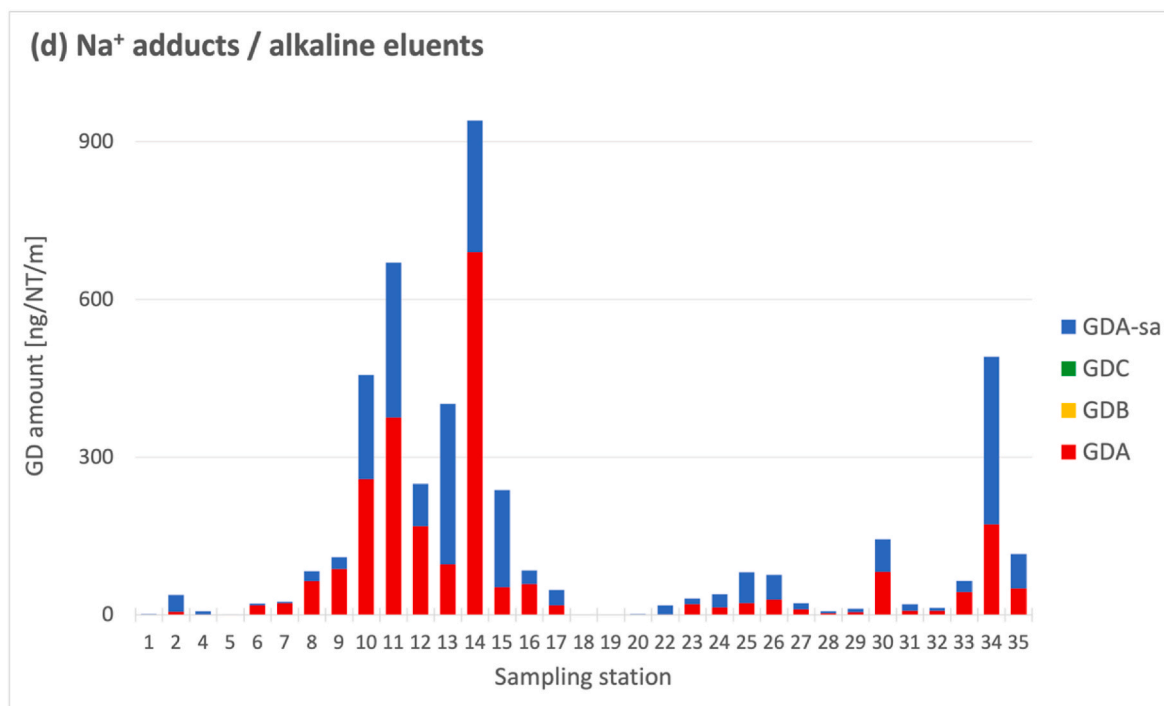
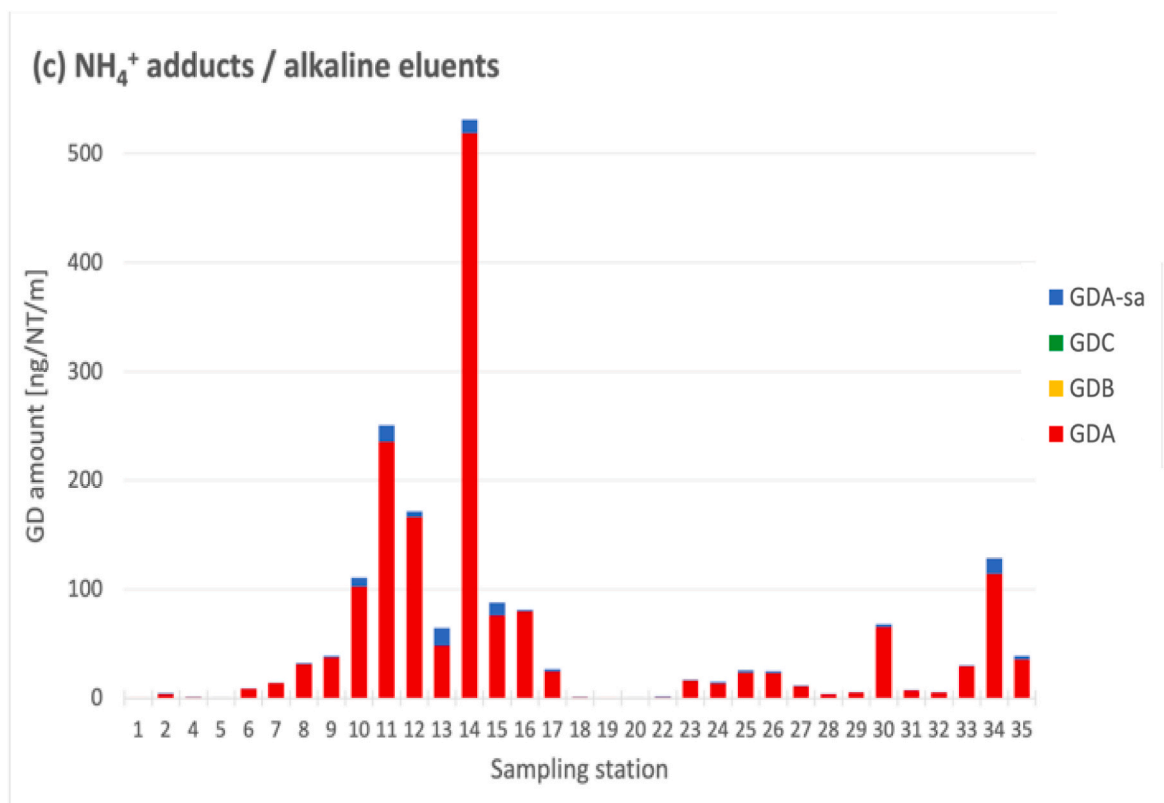


Fig. 6. (continued).

resulting seco acids provides a more straightforward avenue for identification of the structures of the macrocyclic congeners because formation of a fragment ion from the acyclic seco acids requires cleavage of only a single bond.

4.5. Distribution of GDA and GDA-sa between *A. monilatum* cells and laboratory growth medium

We have found that GDA exists predominantly within the *A. monilatum* cell whereas the seco acid form is found predominantly outside the cell. (Fig. 5). Studies with *A. pseudogonyaulax*, *A. hiranoi* and

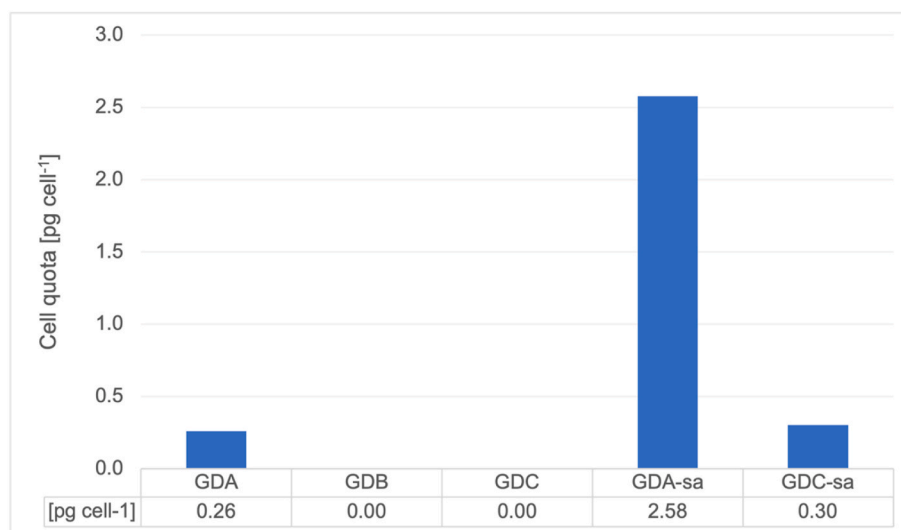
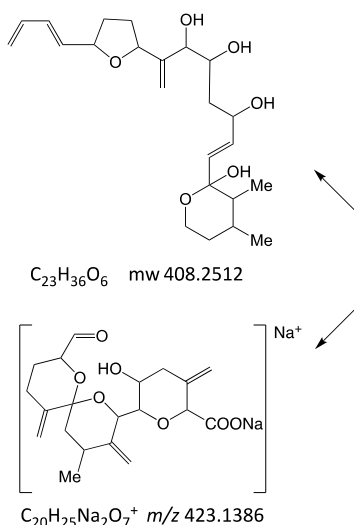
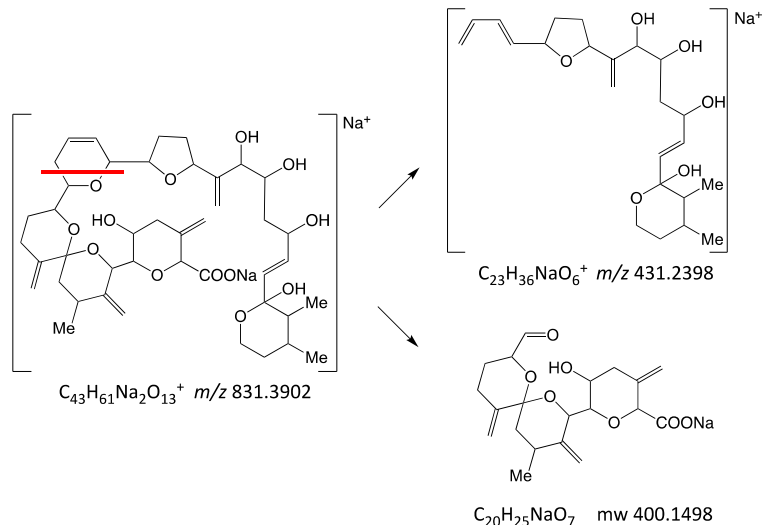


Fig. 7. Extracellular goniiodomin quotas of GDA, GDB, GDC, GDA-sa and GDC-sa from *A. pseudogonyaulax* expressed as GDA equivalents of the NH_4^+ adducts).

If Charge Remains with Head



If Charge Remains with Tail



Scheme 1. Observed retro-Diels-Alder fragmentation of the disodio adduct of seco acid **4b**. Concurrent fragmentations create positive charge on both the head and tail fragments. The red line indicates the site of cleavage.

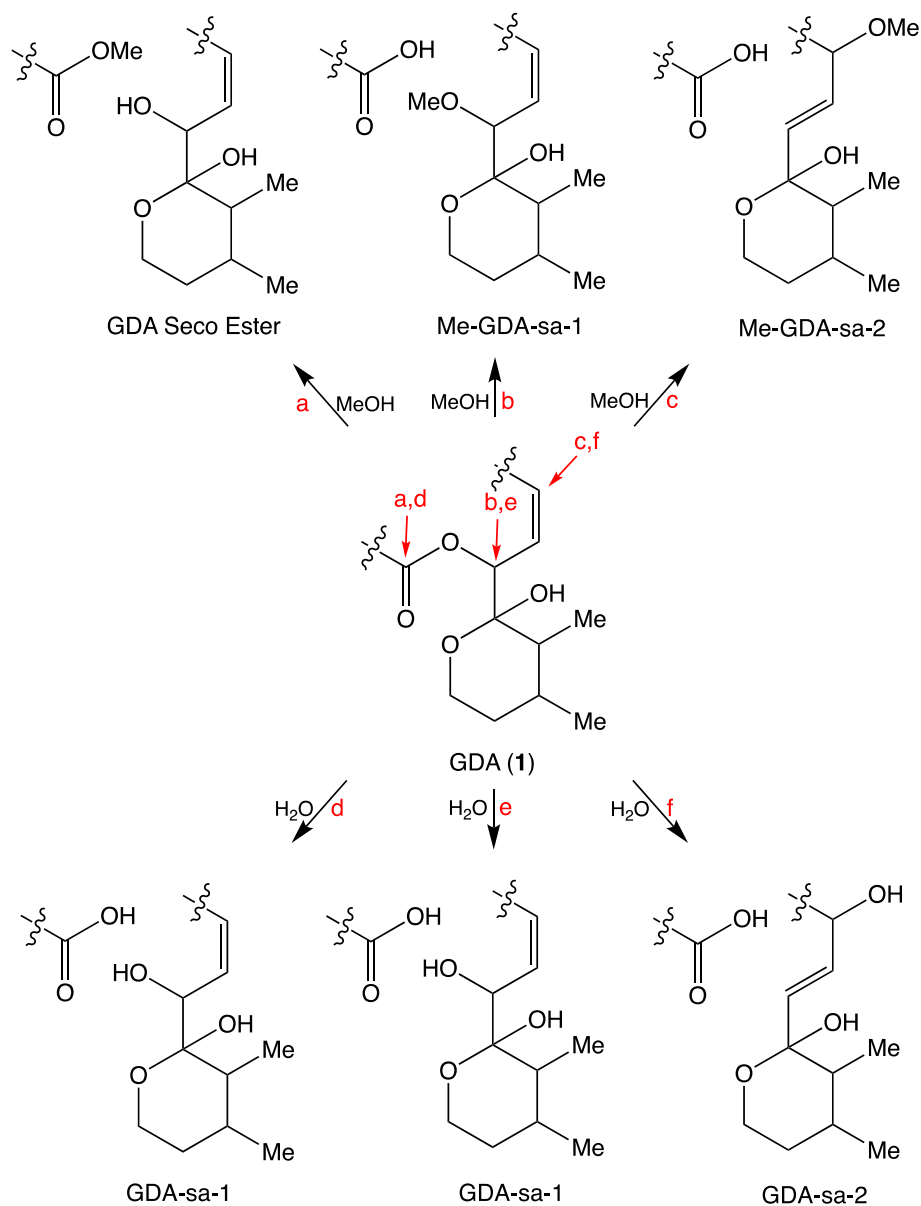
A. taylorii have led to the same conclusion (Hintze, 2021). It seems likely that conversion occurs after GDA has been excreted but further study is needed to establish the sequence of events because Onofrio (2020) observed rapid hydrolysis of GDA in filtered seawater ($t_{1/2} < 6$ h). Extracellular cleavage is promoted by the alkaline pH of the marine environment which is typically ~ 8 . We also observe hydrolysis in seawater although much more slowly than Onofrio reported. Within the cell, the site of GDA storage is unknown but GDA, being a lipophilic compound, is likely to be concentrated in cellular membranes or other lipid-rich regions of the cell.

4.6. Results of the 2020 Limfjord expedition

A. pseudogonyaulax was found to be the dominant *Alexandrium* species in all samples taken and, in parallel, goniiodomins made up the largest proportion of the lipophilic toxins detected in samples from all stations. Additionally, a good correlation was obtained between the cell count of *A. pseudogonyaulax* and the total GD amount per sample (U.

Tillmann, unpublished data). GDA was the major compound in the cellular extracts. The 20 μm mesh fraction accounted for the largest portion of goniiodomins. This was to be expected, as this mesh size retains cells of *A. pseudogonyaulax* which, with the exception of gametes, have a diameter larger than 20 μm . GDA was the main GD in all cellular samples, followed either by GDB or GDA-sa.

A. pseudogonyaulax is a relatively new member of the community of dinoflagellates in the estuaries of northern Denmark, replacing *A. catenella/ostenfeldii* (Kremp et al., 2019). Earlier surveys had revealed that the turnover occurred about 2009. The 2016 sampling expedition had been limited to GDA plus a minor co-metabolite, 34-desMe-GDA (Krock et al., 2018; Harris et al., 2020b). The 2016 expedition was repeated in 2020 to observe possible changes in the distribution of GDA. In addition, with the realization that GDA is readily converted to GDA-sa in the marine environment, a second objective was to determine whether GDA-sa was a major constituent of the mixture of GDs being produced by *A. pseudogonyaulax*. The distribution of GDA in the current survey remained very similar to what had been found in the previous



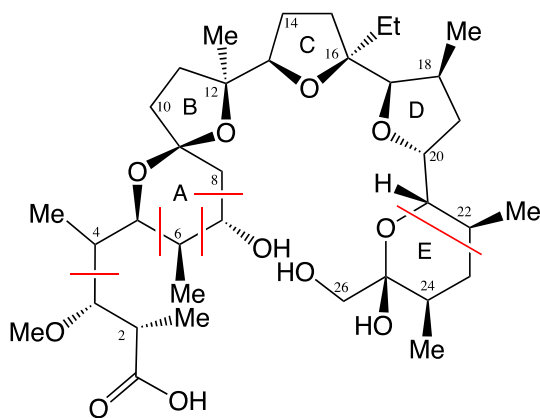
Scheme 2. There are two levels in this scheme with methanolysis on the top and hydrolysis on the bottom. Methanolysis products, i.e., the methyl ester of GDA-sa, Me-GDA-sa-1 and Me-GDA-sa-2, arise by acyl-O and alkyl-O cleavage by paths a, b and c, respectively, on the top. Hydrolysis products GDA-sa-1 and GDA-sa-2 arise by acyl-O and alkyl-O cleavage paths d, e and f on the bottom. Formation of C29 methanolysis and hydrolysis products only occurs via allylic attack (paths c and f).

one (Krock et al., 2018) but the MS results confirmed the importance of GDA-sa. The present study shows that GDA-sa lies primarily in the water column while GDA is found mainly within the algal cells. This result shows the need to assay both intracellular and extracellular content of GDs in future surveys in order to get a full picture of their distribution for GD-producing *Alexandrium* spp. Investigators should be aware that there are difficulties associated with making reliable assays of the relative amounts of intracellular and extracellular toxins. The intracellular toxins are concentrated within the miniscule cells whereas the extracellular toxins are highly diluted by the immense volumes of the water column. A further problem that should be addressed is the need for quantifiable standards of the structurally heterogeneous, dynamic mixtures of GDA-sa isomers. This problem is exacerbated by differences in ionization efficiencies. The ionization efficiencies of Na⁺ adducts of some, possibly all, of the isomeric forms of GDA-sa are much higher than those of the Na⁺ adducts of GDA. Panels b and c of Fig. 6 show a large enhancement in the size of GDA-sa segments of the bar graphs for Na⁺

adducts.

4.7. Comparison of GDA-sa with monensin

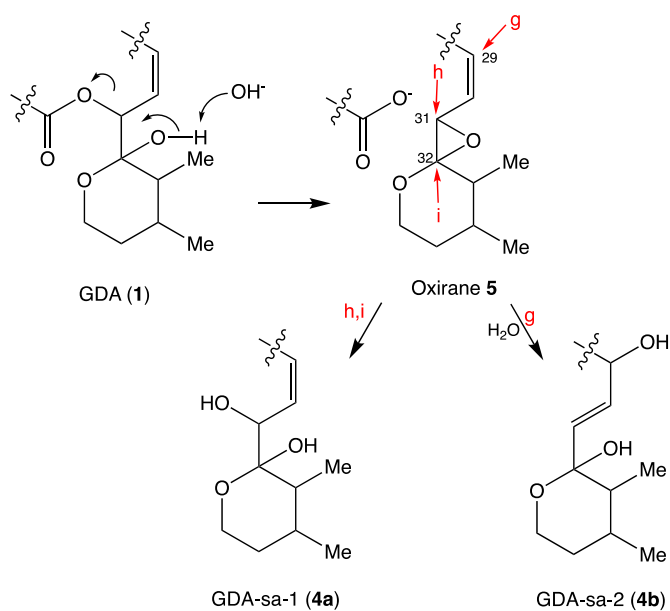
Fragmentation preferences of GDA-sa reported herein can be contrasted with those of monensin A (7), a fungal polyketide carboxylic acid with structural similarities to GDA-sa (Łowicki and Huczyński, 2013). Monensin A lacks the dihydropyran ring which is the basis for retro-Diels-Alder fragmentations of GDA-sa. The only instance where retro-Diels-Alder fragmentation is observed with monensin is in ring E where C22–C23 cleavage occurring after in-source dehydration creates a dihydropyran (Lopes et al., 2002a, b and 2004). CID spectra of monensin are dominated by Grob-Wharton fragmentations occurring at C3–C4, C5–C6, C6–C7 and C7–C8 sites. These are marked in red on structure 6. Fragmentations of monensin can concurrently occur at both ends of the molecule yielding internal fragment ions.



Monensin A (6, Sites of Grob-Wharton fragmentation are marked with red lines)

Monensin A (6, Sites of Grob-Wharton fragmentation are marked with red lines)

Structural similarities of GDA-sa and monensin An appear to extend to their selectivities for complexation with Na^+ and NH_4^+ . [Gertenbach and Popov \(1975\)](#) made a detailed study of complexation of alkali metal ions plus Ag^+ and NH_4^+ with monensin A, finding that the order of complexation is $\text{Ag}^+ > \text{Na}^+ > \text{K}^+ > \text{Rb}^+ > \text{Cs}^+ > \text{Li}^+ \sim \text{NH}_4^+$. They rationalized the sequence of alkali metal ion binding to reflect atomic radii where the radii of Ag^+ and Na^+ were optimal but the radius of Cs^+ was too large and that of Li^+ was too small to make satisfactory fits. They ascribed the weak binding of NH_4^+ to it being too large although its mechanism of complexation is different. The similarities of GDA-sa and monensin A may also extend to their biological properties. Monensin is active against Gram-positive bacteria and is widely used to control coccidiosis in cattle and poultry. The antimicrobial properties of GDA-sa have not yet been investigated but the structural and chemical similarities of GDA-sa and monensin suggest that GDA-sa may play a role in protecting the dinoflagellates from predators. The high efficiency of GDA-sa forming mono and disodio adducts in the ion source suggests that GDA-sa, like monensin, is a sodium ionophore.



Scheme 3. Formation of seco acids 4a and 4b by intramolecular attack of the C32 hydroxy group of GDA at C31 to yield oxirane 5 followed by hydrolysis of 5 b by attack of H_2O at C29, C31 and C32 (Paths g, h and i, respectively).

5. Conclusions

Hydrolysis of the lactone moiety of GDA occurs under extraordinarily mild conditions, even in pure water with the reaction yielding a mixture of 29- and 31-hydroxy seco acids. The seco acids are unstable, undergoing gradual equilibration with conjugated species. This transformation is consistent with opening of the ring F hemiketal and tautomerism yielding α,β -unsaturated ketones. The tautomerism creates dynamic mixtures of structural and configurational isomers which preclude characterization by NMR spectroscopy and X-ray crystallography. High resolution mass spectra with CID fragmentation and HPLC chromatography with UV and MS detection provide evidence for the seco acids being tautomeric and stereoisomeric mixtures involving C31 and nearby atoms.

In laboratory cultures and in the natural environment, GDA exists mainly within the dinoflagellate cells whereas seco acids accumulate in the surrounding medium. Nevertheless, SPATTs can accumulate GDA and from this observation it can be concluded that formation of GDA-sa occurs primarily after GDA has been excreted from the cells. The short lifetime of GDA in the water column and long lifetime of GDA-sa leads to the conclusion that GDA-sa is likely to be the more toxic entity in the natural environment. As a consequence, future studies of the goniodomins should be focused on the acyclic seco acids rather than on GDA and related macrocyclic lactones.

The structural variability of goniodomins is high and has not yet been fully explored. The rich collection of MS fragmentation sites that have been revealed for GDA-sa in the present study will be of much value for probing the structures of the increasing numbers of GDA variants being found as new strains of existing species and new species are discovered ([Harris et al., 2020b](#); [Krock et al., 2018](#)). Use of the fragmentation sites of seco acids for identification of the structures of novel analogs of GDA will be facilitated by the ease with which the GDAs can be converted to the seco acids.

Credit author contribution statement

Constance M. Harris: Investigation, review, visualization and editing. **Luisa Hintze:** Investigation, writing, review, visualization and editing. **Sylvain Gaillard:** Investigation, editing and review. **Simon Tanniou:** Investigation. **Hamish Small:** Investigation, review. **Kimberly S. Reece:** Funding acquisition, resources and editing. **Urban Tillmann:** Methodology, review. **Bernd Krock:** Funding acquisition investigation, methodology, visualization, review. **Thomas M. Harris:** Conceptualization, investigation, methodology, visualization, formal analysis, writing original draft, review and editing.

Ethical statement

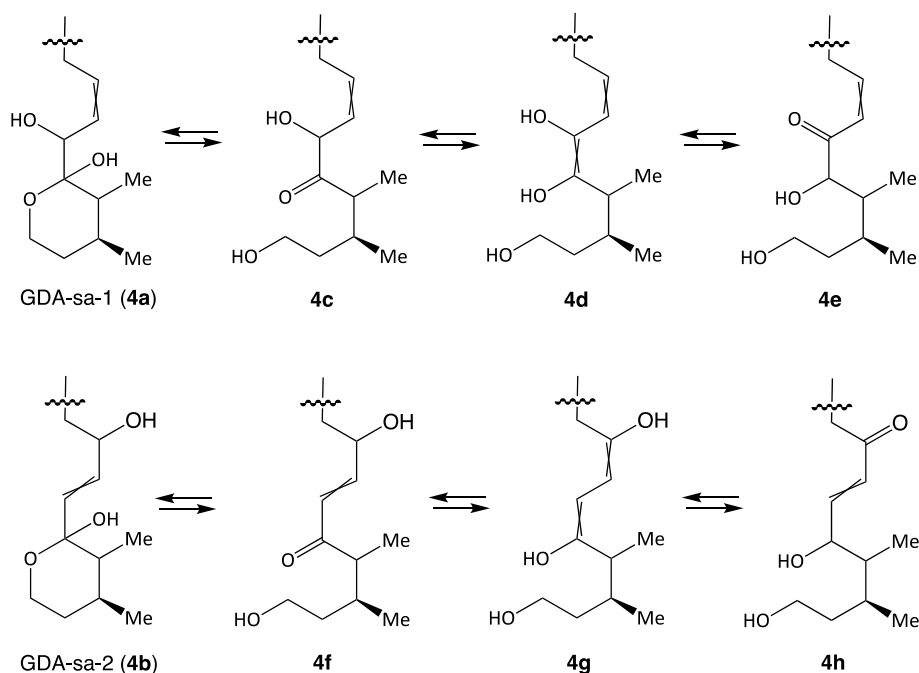
The authors declare to follow the ethics outlined in the Elsevier 'ethics in research and publication procedure'.

Funding

Support for this work was provided by NOAA (ECOHAB grant # NA17NOS4780182) and the Virginia Institute of Marine Science. This work was partly funded by the Alfred Wegener Institute through the Helmholtz initiative "Changing Earth - Sustaining our Future".

Declaration of competing interest

The authors declare that they have no known competing financial interests or personal relationships that could have appeared to influence the work reported in this paper.



Scheme 4. 4a tautomerizes with 4cde; 4b tautomerizes with 4fgh.

Data availability

Data will be made available on request.

Acknowledgements

We are grateful to Isaiah Ruhl (Old Dominion Univ., Norfolk, VA, USA) for high-resolution mass spectra.

References

- Abe, M., Inoue, D., Matsunaga, K., Ohizumi, Y., Ueda, H., Asano, T., Murakami, M., Sato, Y., 2002. Goniiodomin A, an antifungal polyether macrolide, exhibits antiangiogenic activities via inhibition of actin reorganization in endothelial cells. *J. Cell. Physiol.* 190, 109–116.
- Anderson, D.M., Alpermann, T.J., Cembella, A.D., Collos, Y., Masseret, E., Montresor, M., 2012. The globally distributed genus *Alexandrium*: multifaceted roles in marine ecosystems and impacts on human health. *Harmful Algae* 14, 10–35.
- Anon, 2006. Preparation of 0.1 M sodium phosphate buffer at 25 °C. Cold Spring Harb. Protoc. <https://doi.org/10.1101/pdb.tab20>.
- Biemann, K., 1962. Mass Spectrometry: Organic Chemical Applications. McGraw-Hill, New York.
- Borgeat, P., Samuelsson, B., 1979. Arachidonic acid metabolism in polymorphonuclear leukocytes: unstable intermediate in formation of dihydroxy acids. *Proc. Natl. Acad. Sci. USA* 76, 3213–3217.
- Connell, C.H., Cross, J.B., 1950. Mass mortality of fish associated with the protozoan *Gonyaulax* in the Gulf of Mexico. *Science* 112, 359–363.
- Espiña, B., Cagide, E., Louzao, M.C., Vilarinho, N., Vieytes, M.R., Takeda, Y., Sasaki, M., Botana, L.M., 2016. Cytotoxicity of goniiodomin A and B in non contractile cells. *Toxicol. Lett.* 250–251, 10–20.
- Fujiwara, K., Naka, J., Katagiri, T., Sato, D., Kawai, H., Suzuki, T., 2007. Synthesis and relative stereochemistry of the A- and F-rings of goniiodomin A. *Bull. Chem. Soc. Jpn.* 80, 1173–1186.
- Furukawa, K., Sakai, K., Watanabe, S., Maruyama, K., Murakami, M., Yamaguchi, K., Ohizumi, Y., 1993. Goniiodomin A induces modulation of actinomycin ATPase activity mediated through conformational change in actin. *J. Biol. Chem.* 268, 26026–26031.
- Fuwa, H., Nakajima, M., Shi, J., Takeda, Y., Saito, T., Sasaki, M., 2011. A convergent synthesis of the C1–C16 segment of goniiodomin A via palladium-catalyzed organostannane-thioester coupling. *Org. Lett.* 13, 1106–1109.
- Fuwa, H., Matsukida, S., Miyoshi, T., Kawashima, Y., Saito, T., Sasaki, M., 2016. Progress toward the total synthesis of goniiodomin A: stereocontrolled, convergent synthesis of the C12–C36 fragment. *J. Org. Chem.* 81, 2213–2227.
- Gaillard, S., Réveillon, D., Mason, P.L., Ayache, N., Sanderson, M., Smith, J.L., Giddings, S., McCarron, P., Séchet, V., Hégarret, H., Hess, P., Vogelbein, W.K., 2023. Mortality and histopathology in sheepshead minnow (*Cyprinodon variegatus*) larvae exposed to pectenotoxin-2 and *Dinophysis acuminata*. *Aquat. Toxicol.* 257, 106456.
- Gates, J.A., Wilson, W.B., 1960. The toxicity of *Gonyaulax monilata* Howell to *Mugil cephalus*. *Limnol. Oceanogr.* 5, 171–174.
- Gertenbach, P.G., Popov, A.I., 1975. Solution chemistry of monensin and its alkali metal ion complexes. Potentiometric and spectroscopic studies. *J. Am. Chem. Soc.* 97, 4738–4744.
- Guengerich, F.P., Johnson, W.W., Shimada, T., Ueng, Y.-F., Yamazaki, H., Langouët, S., 1998. Activation and detoxification of aflatoxin B₁. *Mutat. Res.* 402 (1998), 121–128.
- Guillard, R.R.L., Hargraves, P.E., 1993. *Stichochrysis immobilis* is a diatom, not a chrysophyte. *Phycologia* 32, 234–236.
- Harding, J.A., Mann, R., Moeller, P., Hsia, M.E., 2009. Mortality of the veined rapa whelk, *Rapana venosa*, in relation to a bloom of *Alexandrium monilatum* in the York River, United States. *J. Shellfish Res.* 28, 363–367.
- Harris, C.M., Reece, K.S., Stec, D.F., Scott, G.P., Jones, W.M., Hobbs, P.L.M., Harris, T.M., 2020a. The toxin goniiodomin, produced by *Alexandrium* spp., is identical to goniiodomin A. *Harmful Algae* 92, 101707.
- Harris, C.M., Reece, K.S., Harris, T.M., 2020b. Revisiting the toxin profile of *Alexandrium pseudogonyaulax*; formation of a desmethyl congener of goniiodomin. *A. Toxicol* 188, 122–126.
- Harris, C.M., Krock, B., Tillmann, U., Tainter, C.J., Stec, D.F., Andersen, A.J.C., Larsen, T.O., Reece, K.S., Harris, T.M., 2021. Alkali metal and acid-catalyzed interconversion of goniiodomin A with congeners. *J. Nat. Prod.* 84, 2554–2567.
- Hess Jr., B.A., Smentek, L., 2022. Mechanisms of the aqueous solvolysis of the ring-opening of the lactone ring of goniiodomin A. *Int. Res. J. Pure Appl. Chem.* 23, 9–16.
- Hintze, L., 2021. M.S. Thesis. University of Applied Sciences, Mannheim, Germany. Remove extra line below this reference.
- Howell, J.F., 1953. *Gonyaulax monilata*, sp. nov., the causative dinoflagellate of a red tide on the east coast of Florida in Aug.–Sept., 1951. *Trans. Am. Microsc. Soc.* 72, 153–156.
- Hsia, M.H., Morton, S.L., Smith, L.L., Beauchesne, K.R., Huncik, K.M., Moeller, P.D.R., 2006. Production of goniiodomin A by the planktonic, chain-forming dinoflagellate *Alexandrium monilatum* (Howell) Balech isolated from the gulf coast of the United States. *Harmful Algae* 5, 290–299.
- Katagiri, T., Fujiwara, K., Kawai, H., Suzuki, T., 2008a. Synthesis of the DE-ring of goniiodomin A and prediction of its natural relative stereochemistry. *Tetrahedron Lett.* 49, 233–237.
- Katagiri, T., Fujiwara, K., Kawai, H., Suzuki, T., 2008b. Synthesis of the ABC-ring models of goniiodomin A: preference for the unnatural configuration at C11 of the BC-ring in a non-macrocyclic model system. *Tetrahedron Lett.* 49, 3242–3247.
- Kawashima, Y., 2018. Studies toward the Total Synthesis of Amphidinolide N and Goniiodomin A. Ph.D. Dissertation (Abstract). Tohoku Univ., Sendai, Japan. <http://hdl.handle.net/10097/00122676>.
- Keller, M.D., Selvin, R.C., Claus, W., Gaillard, R.R.L., 1987. Media for the culture of oceanic ultraphytoplankton. *J. Phycol.* 23, 633–638.
- Kilham, S.S., Kreger, D.A., Lynn, S.G., Goulden, C.E., Herrera, L., 1998. COMBO: a defined freshwater culture medium for algae and zooplankton. *Hydrobiologia* 377, 147–159.
- Kremp, A., Hansen, P.J., Tillmann, U., Savela, H., Suikkanen, S., Voß, D., Barrera, F., Jakobsen, H.H., Krock, B., 2019. Distributions of three *Alexandrium* species and their toxins across a salinity gradient suggest an increasing impact of GDA producing

- A. pseudogonyaulax* in shallow brackish waters of Northern Europe. *Harmful Algae* 67, 101622.
- Krock, B., Tillmann, U., Wen, Y., Hansen, P.J., Larsen, T.O., Andersen, A.J.C., 2018. Development of a LC-MS/MS method for the quantification of goniodomins A and B and its application to *Alexandrium pseudogonyaulax* strains and plankton field samples of Danish coastal waters. *Toxicon* 155, 51–60.
- Long, M., Krock, B., Castrec, J., Tillmann, U., 2021. Unknown extracellular and bioactive metabolites of the genus *Alexandrium*: a review of overlooked toxins. *Toxins* 13, 905.
- Lopes, N.P., Stark, C.B.W., Hong, H., Gates, P.J., Staunton, J., 2002a. Fragmentation studies on monensin A and B by accurate-mass electrospray tandem mass spectrometry. *Rapid Commun. Mass Spectrom.* 16, 414–420.
- Lopes, N.P., Stark, C.B.W., Gates, P.J., Staunton, J., 2002b. Fragmentation studies on monensin A by sequential mass spectrometry. *Analyst* 127, 503–506.
- Lopes, N.P., Stark, C.B.W., Staunton, J., Gates, P.J., 2004. Evidence for gas-phase redox chemistry inducing novel fragmentation in a complex natural product. *Org. Biomol. Chem.* 2, 358–363.
- Łowicki, D., Huczynski, A., 2013. Structure and antimicrobial properties of monensin A and its derivatives: summary of the achievements. *BioMed Res. Int.* 742149.
- Ma, H., Krock, B., Tillmann, U., Cembella, A., 2009. Preliminary characterization of extracellular allelochemicals of the toxic marine dinoflagellate *Alexandrium tamarense* using a *Rhodomonas salina* bioassay. *Mar. Drugs* 7, 497–522.
- MacKenzie, L., Beuzenberg, V., Holland, P., McNabb, P., Selwood, A., 2004. Solid phase adsorption toxin tracking (SPATT): a new monitoring tool that simulates the biotoxin contamination of filter feeding bivalves. *Toxicon* 44, 901–918.
- Matsunaga, K., Nakatani, K., Murakami, M., Yamaguchi, K., Ohizumi, Y., 1999. Powerful activation of skeletal muscle actomyosin ATPase by goniiodomin A is highly sensitive to troponin/tropomyosin complex. *J. Pharmacol. Exp. Therapeut.* 291, 1121–1126.
- May, S.P., Burkholder, J.M., Shumway, S.E., Hégaret, H., Wikfors, G.H., 2010. Effects of the toxic dinoflagellate *Alexandrium monilatum* on survival, grazing and behavioral response of three ecologically important bivalve molluscs. *Harmful Algae* 9, 281–293.
- Mizuno, K., Nakahata, N., Ito, E., Murakami, M., Yamaguchi, K., Ohizumi, Y., 1998. Goniiodomin A, an antifungal polyether macrolide, increases the filamentous actin content of 1321N1 human astrocytoma cells. *J. Pharm. Pharmacol.* 50, 645–648.
- Murakami, M., Makabe, K., Yamaguchi, K., Konosu, S., Wälchli, M.R., 1988a. Goniiodomin A, a novel polyether macrolide from the dinoflagellate *Goniodoma pseudogoniaulax*. *Tetrahedron Lett.* 29, 1149–1152.
- Murakami, M., Okita, Y., Matsuda, H., Okino, T., Yamaguchi, K., 1998b. From the dinoflagellate *Alexandrium hiranoi*. *Phytochemistry* 48, 85–88.
- Murphy, R.C., 2014. Tandem mass spectrometry of lipids; molecular analysis of complex lipids (Cambridge, U.K). *New developments in mass spectrometry*; Chapt 1, 1–39.
- Nakajima, M., 2014. *Synthetic Study of Goniiodomin A*. Ph.D. Dissertation. Tohoku Univ., Sendai, Japan (abstract). <http://hdl.handle.net/10097/58723>.
- Onofrio, M.D., Mallet, C.R., Place, A.R., Smith, J.L., 2020. A screening tool for the direct analysis of marine and freshwater phycotoxins in organic SPATT extracts from the Chesapeake Bay. *Toxins* 12, 322.
- Onofrio, M.D., 2020. *Spatial and Temporal Distribution of Phycotoxins in Chesapeake Bay: Method Development and Application*. M.S. Thesis. William & Mary, Virginia Institute of Marine Science.
- Patiny, L., Borel, A., 2013. ChemCalc: a building block for tomorrow's chemical infrastructure. *J. Chem. Inf. Model.* 53, 1223–1238.
- Rickborn, B., 1998a. The retro-diels-alder reaction. Part I. C–C dienophiles. *Org. React.* 52, 1–393.
- Rickborn, B., 1998b. The retro-Diels-Alder reaction. Part II. Dienophiles with one or more heteroatoms. *Org. React.* 53, 223–629.
- Saito, T., Fuwa, H., Sasaki, M., 2009. Toward the total synthesis of goniiodomin A, an actin-targeting marine polyether macrolide: convergent synthesis of the C15–C36 segment. *Org. Lett.* 11, 5274–5277.
- Sharma, G.M., Michaels, L., Burkholder, P.R., 1968. Goniiodomin, a new antibiotic from a dinoflagellate. *J. Antibiot. (Tokyo)* 21, 659–664.
- Smith, J.L., Tong, M., Kulis, D., Anderson, D.M., 2018. Effect of ciliate strain, size, and nutritional content on the growth and toxicity of mixotrophic *Dinophysis acuminata*. *Harmful Algae* 78, 95–105.
- Tainter, C.J., Schley, N.D., Harris, C.M., Stec, D.F., Song, A.K., Balinski, A., May, J.C., McLean, J.A., Reece, K.S., Harris, T.M., 2020. Algal toxin goniiodomin A binds potassium ion selectively to yield a conformationally altered complex with potential biological consequences. *J. Nat. Prod.* 83, 1069–1081.
- Takeda, Y., Shi, J., Oikawa, M., Sasaki, M., 2008. Assignment of the absolute configuration of goniiodomin A by NMR spectroscopy and synthesis of model compounds. *Org. Lett.* 10, 1013–1016.
- Tillmann, U., Krock, B., Wietkamp, S., Beran, A., 2020. A Mediterranean *Alexandrium taylorii* (Dinophyceae) strain produces goniiodomin A and lytic compounds but not paralytic shellfish toxins. *Toxins* 12, 564.
- Tillmann, U., John, U., 2002. Toxic effects of *Alexandrium* spp. on heterotrophic dinoflagellates: an allelochemical defence mechanism independent of PSP-toxin content. *MEPS* 230, 47–58.
- Tureček, F., Hanuš, V., 1984. Retro-Diels-Alder reaction in mass spectrometry. *Mass Spectrom. Rev.* 3, 85–152.
- Yasuda, M., Nakatani, K., Matsunaga, K., Murakami, M., Momose, K., Ohizumi, Y., 1998. Modulation of actinomycin ATPase by goniiodomin A differs in types of cardiac myosin. *Eur. J. Pharmacol.* 346, 119–123.
- Zmerli Triki, H., Laabir, M., Moeller, P., Chomérat, N., Daly-Yahia, O.K., 2016. First report of goniiodomin A production by the dinoflagellate *Alexandrium pseudogonyaulax* developing in southern Mediterranean (Bizerte Lagoon, Tunisia). *Toxicon* 111, 91–99.